ELSEVIER

LITHOS

An International Journal of Petrology,
Geochemistry and Mineralogy

VOLUME 113, Nos. 3–4
DECEMBER 2009
ISSN 0024-4937

www.elsevier.com/locate/lithos

A geochemical and Sr–Nd isotopic study of the Vendian greenstones from Gorny Altai, southern Siberia: Implications for the tectonic setting of the formation of greenstones and the role of oceanic plateaus in accretionary orogen

Atsushi Utsunomiya [a],*, Bor-ming Jahn [a], Tsutomu Ota [b], Inna Yu. Safonova [c]

[a] Institute of Earth Sciences, Academia Sinica, Academia Road 2-128, Nankang, Taipei 11529, Taiwan
[b] Institute of Study of the Earth's Interior, Okayama University, Misasa, Tottori 682-0193, Japan
[c] Institute of Geology and Mineralogy, Siberian Branch of the Russian Academy of Sciences, Koptyuga ave. 3, 630090, Novosibirsk, Russia

ARTICLE INFO

ABSTRACT

The Central Asian Orogenic Belt is considered to be the most important site of juvenile crustal formation since the Neoproterozoic. Gorny Altai of southern Siberia represents the first stage of tectonic evolution in the Central Asian Orogenic Belt. Greenstones of Gorny Altai occur either as blocks within an accretionary complex surrounded by a sedimentary/serpentinite matrix, or as a coherent ophiolite complex. The greenstones are overlain or intercalated by micritic limestones indicating that they formed in shallow water in an intra-oceanic environment. The phenocryst assemblage of the greenstones (clinopyroxene + plagioclase, plagioclase and clinopyroxene) is, however, different from that of mid-oceanic ridge basalt (MORB).

Based on the geochemical characteristics, these greenstones are divided into four groups. Group 1 greenstones show light rare earth element (LREE) depletion but no negative Nb–Ta anomaly in primitive mantle normalized multi-element plots; they resemble normal (N-) MORB or back-arc-basin basalt (BABB). Group 2 rocks have slight LREE depletion or show flat REE patterns; they have a negative Nb–Ta anomaly and are similar to island arc basalt (IAB) or BABB. Group 3 rocks have LREE-enriched patterns, no negative Nb–Ta anomaly and are similar to enriched (E-) MORB or oceanic island basalt (OIB). Group 4 greenstones are represented by LREE-enriched patterns, with negative Nb–Ta anomaly; they resemble IAB. Although the co-existence of such heterogeneous geochemical signatures may suggest that the rocks were formed in different tectonic settings followed by tectonic mixing and aggregation in a subduction zone, the field relationships, petrological and mineralogical composition, and geochemical characteristics suggest that the greenstones were formed as part of an oceanic plateau generated by a mantle plume source which contained a recycled crustal component. An important implication is that oceanic plateaus may represent an important constituent in the development of accretionary orogens.

© 2009 Elsevier B.V. All rights reserved.

1. Introduction

The Central Asian Orogenic Belt encompasses a large area from the Urals in the west, through Kazakhstan, Northwest China, Mongolia, and Northeast China to the Okhotsk Sea in the Russian Far East. It resulted from amalgamation of voluminous subduction–accretionary complexes of Late Neoproterozoic to Mesozoic age (e.g., Sengör et al., 1993; Sengör and Natal'in, 1996). The Central Asian Orogenic Belt is the largest site of juvenile crustal formation during the Phanerozoic (e.g., Kovalenko et al., 2004; Jahn, 2004; Jahn et al., 2000, 2004).

The Gorny Altai region in southern Siberia is one of the key areas for the reconstruction of the tectonic evolution of the Central Asian Orogenic Belt. The region contains well-preserved Late Neoproterozoic to Early Cambrian subduction–accretion complexes formed prior to the Late Paleozoic collision between Siberia and Kazakhstan (Buslov et al., 1993; Buslov and Watanabe, 1996; Buslov et al., 1998, 2001). Greenstone–limestone complexes are distributed throughout the region (Fig. 1) and have geochemical characteristics of mid-ocean ridge basalt (MORB) or oceanic island basalt (OIB; Dobretsov et al., 2004; Safonova et al., 2004). However, the tectonic setting(s) of the basaltic rocks is unclear. In this paper, we use geochemical and isotopic data, supplemented by field geology and petrologic studies, to reassess the tectonic setting(s) and origin of the greenstones.

2. Geological outline

The Gorny Altai region encompasses three fault-bounded tectonic units: the Altai–Mongolian terrane to the southwest, the Gorny Altai

---
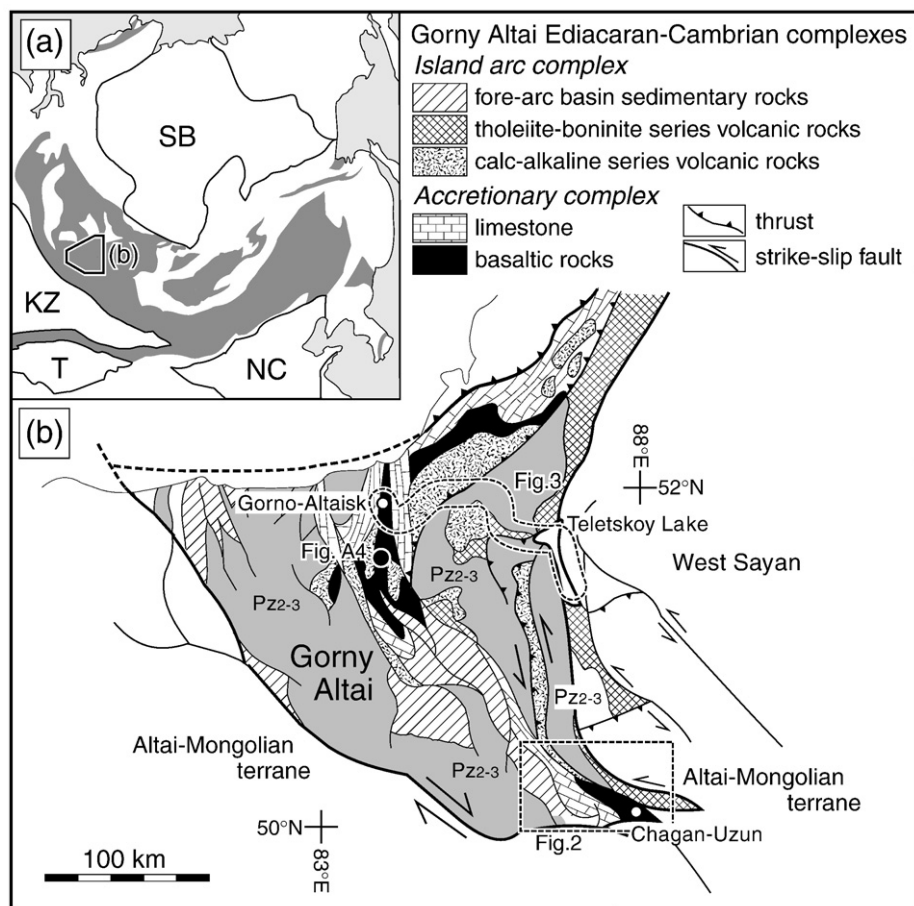
Fig. 1. (a) Index map of subduction–accretion complexes (grey) of the Central Asian Orogenic Belt, which is surrounded by the Siberian (SB), Kazakhstan (KZ), North China (NC) and Tarim (T) continental blocks (modified after Sengör and Natal'in, 1996). (b) Geological sketch map of the Gorny Altai region (modified after Buslov et al., 1993, 2002, 2004). Pz_{2-3} (grey); Middle to Late Paleozoic unit. Localities of Figs. 2, 3 and A4 are shown.

terrane in the center and the West Sayan terrane to the east (Fig. 1). The northern extension of Gorny Altai region is covered by Quaternary sediments. The Altai–Mongolian and West Sayan terranes are intra-oceanic arc systems built with micro-continent blocks within the Paleo-Asian Ocean. They were developed contemporaneously with that of the Gorny Altai terrane (Buslov et al., 2004). The Altai–Mongolian and West Sayan terranes docked with the Gorny Altai terrane in the Late Paleozoic, giving rise to the western segments of the Central Asian Orogenic Belt between Siberia and Kazakhstan (Buslov et al., 2001, 2002, 2003, 2004).

The Gorny Altai subduction–accretion complex represents a piled nappe structure composed, in ascending order, of (1) a Vendian–Cambrian accretionary complex, (2) a Vendian high-P/T meta-morphic complex, (3) an ophiolitic complex, and (4) a Vendian–Cambrian island arc complex (Figs. 2 and 3; Ota et al., 2007). The accretionary, high-P/T metamorphic and ophiolitic complexes are unconformably overlain by Ordovician–Devonian fore-arc sedimen-tary rocks. Later extensional and sinistral strike–slip faults dismem-bered the pre-existing nappe structure which was subsequently covered by Ordovician–Devonian sedimentary rocks along the present NW–SE oriented structures in Gorny Altai (Buslov et al., 1993, 2001; Dobretsov et al., 1995). In the accretionary complex, Vendian-type stromatolites occur with microphyrites, calcareous algae and sponge spicules in limestones, whereas calcareous mudstones adjacent to the limestones have Early Cambrian sponge spicules (Terleev, 1991). A whole-rock Pb–Pb isochron age of 598 ± 25 Ma was determined for the limestone immediately above the

greenstones (Uchio et al., 2004). $^{40}K-^{39}Ar$ ages of 535 to 567 Ma (Buslov and Watanabe, 1996) and $^{40}Ar-^{39}Ar$ plateau ages between 627 and 636 Ma (Buslov et al., 2001, 2002) were obtained for amphiboles in eclogite of the high-P/T metamorphic complex. Buslov and Watanabe (1996) reported a $^{40}K-^{39}Ar$ age of 523 ± 23 Ma for hornblendes separated from an amphibolite in the ophiolitic complex. Therefore, the eruption of the greenstone protoliths most likely occurred at ~600 Ma or earlier. If the eclogites represent an exhumed, subducted greenstone, then they formed before ~640 Ma.

3. Field occurrence of the greenstones

3.1. The accretionary complex

In the southern Gorny Altai terrane (Fig. 2), the accretionary complex is metamorphosed to a low grade and comprises two distinct units: limestone-dominant and basalt-dominant units. In the Kurai area, the limestone-dominant unit is composed mostly of limestone with a minor amount of basaltic blocks (Figs. 4 and A1 online). Near Chagan-Uzun village, limestones with minor chert occur as large exotic blocks in a matrix of cataclastic serpentinite (Fig. A2 online). The serpentinite matrix is weakly foliated along the margins of the blocks, but is clearly less recrystallized than the serpentine (antigorite) schist in the high-P/T metamorphic complex. In the basalt-dominant unit of Kurai, clastic rocks surround blocks of basaltic rocks, micritic limestone, and a small amount of chert (Fig. 4). The basaltic rocks are mostly massive but
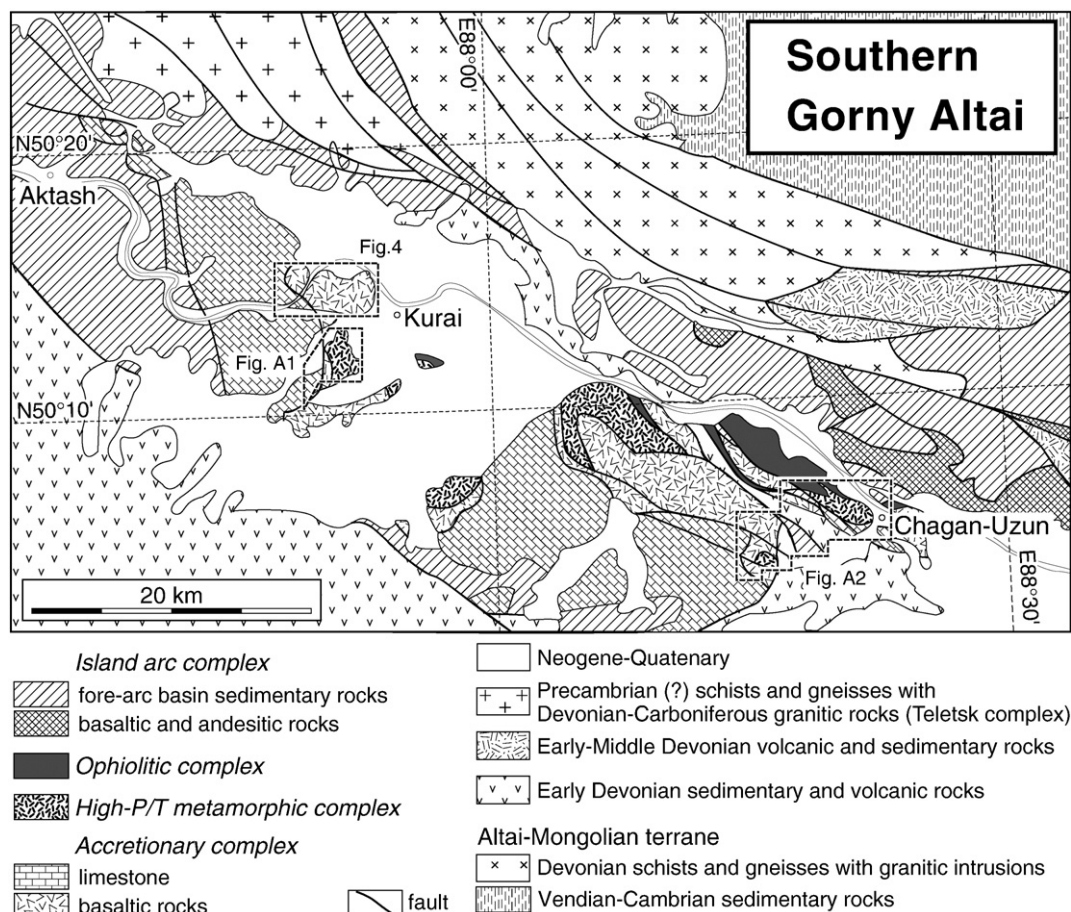
Fig. 2. Geological sketch map of the southern Gorny Altai region (modified after Buslov et al., 1993, 2002 and 2004). Localities of Figs. 4, A1 and A2 are shown.

occasionally have preserved pillow structures indicating a submarine eruption. Both the blocks and their matrix are sheared, and folded with randomly-oriented foliations (Ota et al., 2007). However, in some well-preserved blocks, the basaltic rocks are covered by limestone and the inter-pillow space is filled with micritic limestone (Uchio et al., 2004). In the Chagan-Uzun area, the limestones in the basalt-dominant unit include laminated limestone, bedded micritic limestone, limestone breccia and massive limestone. Massive and bedded limestones often show a depositional contact with underlying basaltic lavas (Uchio et al., 2004). The limestones mostly consist of pure carbonate and do not contain coarse-grained terrigenous (quartzo–felspathic) clastic materials. The clastic rocks are comprised of fragments of pelagic materials, island arc and high-P/T metamorphic complexes (Ota et al., 2007).

In northern Gorny Altai, the accretionary complex consists of low-grade metamorphosed basalt, limestone, mudstone, and minor amount of chert, sandstone and shale (Fig. 3). These rocks occur as several fault-bounded slices (Ota et al., 2007). Within individual units, basaltic rocks are directly covered by limestones. The limestones are bedded, micritic, and interbedded with thin chert layers. Both basalt and limestone are in contact with the surrounding sedimentary rocks (Ota et al., 2007). The occurrence of the greenstones from both the southern and northern regions is similar. The petrological characteristics of the limestones, such as the absence of terrigenous clastic materials, suggest that the limestones were deposited on or near a mid-oceanic topographic high (Uchio et al., 2004). The block-in-matrix relationship of the basalts, limestones and clastic sediments suggests that secondary

mixing of the mid-oceanic (e.g., oceanic island, oceanic plateau, or seamount) rocks and continent- or arc-derived terrigenous clastics probably occurred in an active trench (Isozaki 1997; Ota et al., 2007).

3.2. The high-P/T metamorphic complex

The high-P/T metamorphic complex near Chagan-Uzun village occurs as a subhorizontal thrust sheet bounded by low-angle faults. The peridotite unit of the ophiolitic complex is overlying the high-P/T complex which is underlain by the serpentinite and limestone blocks of the accretionary complex (Fig. A2 online; Ota et al., 2007). The high-P/T metamorphic complex is composed of well-recrystallized and well-foliated serpentinite (antigorite schist), with lenticular intercalations of metabasites and pelitic, calcareous and siliceous schists. The metabasites include eclogite, garnet–amphibolite, amphibolite and lower-grade mafic schist. The schists are highly deformed in tight folds at various scales. In the southwest of Chagan-Uzun, the high-P/T metamorphic complex is composed of low-grade mafic schist with small lenses of siliceous and calcareous schists. It occurs as a slab, separated by a low-angle fault from the underlying basaltic rocks of the accretionary complex. The high-P/T metamorphic complex also occurs at Kurai and has a similar lithology to that in the southwest of Chagan-Uzun (Fig. A1 online). The metabasites in these two localities frequently preserve igneous textures, suggesting their protoliths were basaltic lavas and clastics, and dolerites.
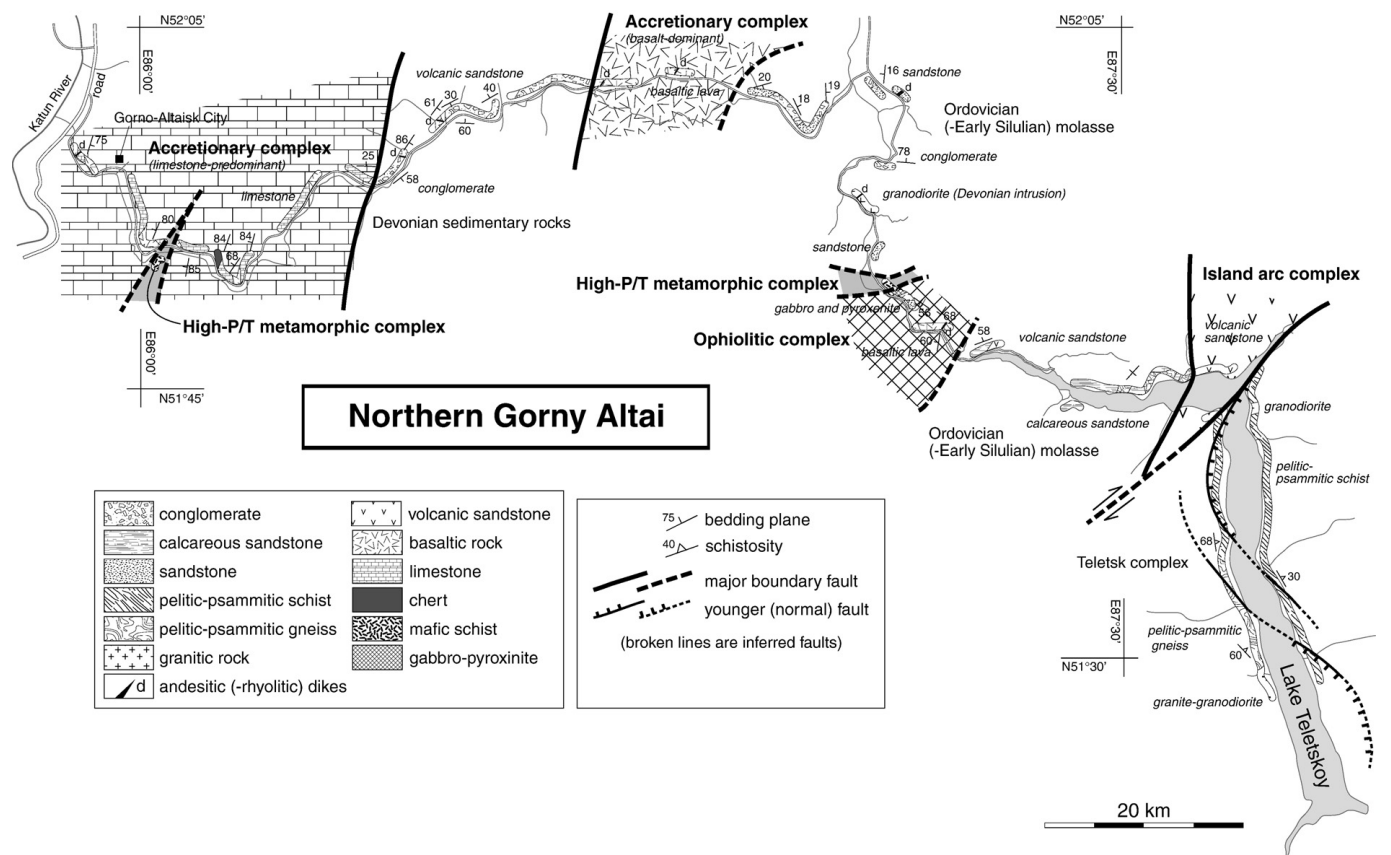
Fig. 3. Geotraverse of the northern Gorny Altai region between Gorno-Altaisk and Lake Teletskoy (Ota et al., 2007).
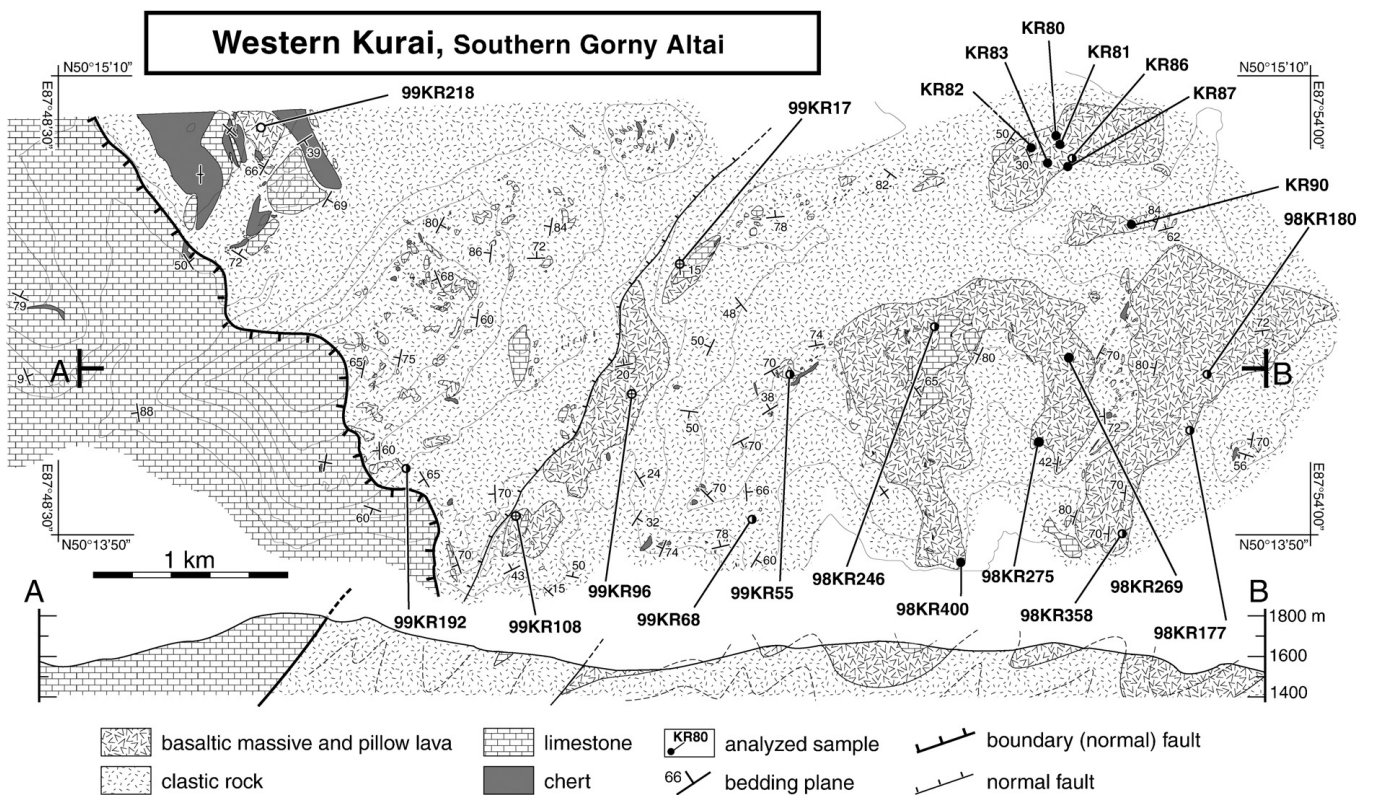
Fig. 4. Geological map and profile of western Kurai, southern Gorny Altai region (Ota et al., 2007). Sample localities are shown. Solid = Group 1; half solid = Group 2; open = Group 3; with cross = Group 4. The sample grouping is described in Section 7.2.

Table 1
Representative major and trace element compositions of greenstones from southern Gorny Altai.

Sample	KR80[a,b]	KR81[a,b]	KR82[a,b]	KR83[a,b]	KR86[a,b]	KR87[a,b]	KR90[a,b]	98KR177[b]	98KR269[b]	98KR400[b]	99KR17[b]	99KR68[b]
Area	W. Kurai	W. Kurai	W. Kurai	W. Kurai	W. Kurai	W. Kurai	W. Kurai	W. Kurai	W. Kurai	W. Kurai	W. Kurai	W. Kurai
Complex	AC	AC	AC	AC	AC	AC	AC	AC	AC	AC	AC	AC
Lithology	Basalt	Basalt	Basalt	Dolerite	Basalt	Basalt	Basalt	Basalt	Basalt	Basalt	Basalt	Basalt
Group	1	1	1	1	2	1	1	2	1	1	4	2
(wt.%)												
SiO_2	48.23	47.57	49.22	48.69	49.59	50.76	49.73	55.13	49.03	50.56	46.35	47.89
TiO_2	2.03	1.64	2.05	2.42	1.02	2.07	1.68	1.62	2.03	1.84	1.94	1.66
Al_2O_3	14.22	12.52	14.24	14.39	15.15	16.36	13.84	12.92	13.41	13.31	15.84	13.68
Fe_2O_3	13.44	12.23	13.39	14.53	11.91	11.61	11.81	11.93	12.97	11.90	14.85	14.14
MnO	0.21	0.19	0.21	0.24	0.22	0.21	0.45	0.19	0.22	0.20	0.25	0.20
MgO	6.19	8.24	6.05	4.91	5.27	4.35	6.04	3.77	5.77	5.20	7.29	4.65
CaO	8.73	9.41	8.79	7.47	9.09	8.07	8.30	6.55	9.35	9.68	4.03	11.36
Na_2O	3.55	2.53	3.92	3.88	5.15	5.00	5.27	4.24	3.16	3.95	3.58	2.60
K_2O	0.21	0.48	0.21	1.45	0.03	0.45	0.12	0.05	0.24	0.00	0.27	0.01
P_2O_5	0.22	0.17	0.23	0.25	0.10	0.25	0.18	0.08	0.18	0.16	0.41	0.07
LOI	4.19	5.62	2.18	2.79	3.97	2.21	3.71	2.07	2.37	1.85	5.02	2.99
Total	101.22	100.62	100.49	101.02	101.50	101.33	101.13	98.55	98.73	98.64	99.83	99.25
(ppm)												
P	916	732	985	1071	415	1147	803	512	919	926	1923	478
Sc	37.3	46.0	35.6	34.8	31.8	33.9	37.9	36.6	38.6	36.9	27.2	38.7
V	349	321	349	384	308	328	333	464	343	327	319	502
Cr	131	385	120	29	56	45	150	20	101	102	4	25
Co	41.1	43.5	46.5	43.3	44.8	42.3	43.2	25.5	38.4	36.6	26.7	34.0
Ni	50.9	109.4	51.1	21.0	27.4	31.2	52.1	11.9	47.9	44.6	13.5	16.9
Cu	69.2	96.2	68.4	10.5	134.1	52.4	82.7	23.7	59.2	57.9	61.4	34.3
Zn	109	112	123	92	79	113	110	89	121	100	56	101
Ga	19	17	19	20	16	18	16	15	21	19	20	20
Ge	1.5	1.3	1.4	1.6	1.2	1.3	1.3	1.4	1.6	1.6	1.8	1.7
As	0.7	0.5	1.3	0.6	1.5	1.2	0.6	0.3	1.2	0.8	0.6	0.5
Se	0.10	0.09	0.12	0.09	0.07	0.11	0.09	0.07	0.11	0.12	0.06	0.07
Rb	7.4	6.3	3.6	10.7	0.4	4.6	1.9	1.1	2.6	0.3	6.0	0.8
Sr	292	240	190	132	84	354	255	78	156	72	301	94
Y	42.4	37.4	51.0	39.2	22.0	48.9	39.7	27.8	48.9	48.6	26.4	27.5
Zr	148	116	165	129	48	173	118	60	155	149	85	56
Nb	3.25	2.53	3.62	4.06	0.81	3.70	2.41	0.84	3.37	3.36	3.24	0.76
Mo	1.22	1.16	0.51	0.55	0.73	0.47	0.56	1.04	1.31	1.14	0.55	0.38
Sn	0.54	2.04	0.90	0.15	0.47	0.46	1.05	0.09	0.80	1.72	0.67	0.66
Sb	1.26	1.46	0.69	0.04	0.50	0.08	0.48	0.05	0.15	0.03	0.12	0.16
Cs	1.61	1.12	0.32	0.54	0.09	0.29	0.18	0.39	0.18	0.07	1.38	0.19
Ba	125	92	95	233	28	252	129	14	47	8	333	18
La	5.00	4.56	6.29	5.39	1.82	6.33	4.34	3.20	6.08	5.91	7.29	2.84
Ce	15.67	13.38	19.56	16.22	5.51	19.69	13.31	9.06	18.22	17.86	19.15	8.03
Pr	2.65	2.19	3.25	2.64	0.93	3.25	2.22	1.50	3.01	2.91	2.82	1.34
Nd	14.93	12.22	17.53	14.64	5.52	17.77	12.43	8.47	16.43	16.11	14.52	7.50
Sm	5.08	4.19	5.90	4.88	2.05	5.83	4.24	2.92	5.55	5.44	4.21	2.69
Eu	1.63	1.40	1.87	1.68	0.76	1.71	1.30	1.01	1.85	1.67	1.36	1.06
Gd	6.03	4.96	6.98	5.66	2.54	6.86	5.09	3.70	6.87	6.67	4.66	3.45
Tb	1.24	1.04	1.44	1.15	0.54	1.41	1.07	0.75	1.37	1.33	0.83	0.70
Dy	8.11	6.89	9.43	7.31	3.54	9.16	7.00	4.87	8.85	8.68	4.92	4.61
Ho	1.76	1.51	2.08	1.59	0.79	2.01	1.54	1.07	1.94	1.91	1.02	1.02
Er	4.89	4.26	5.86	4.44	2.20	5.76	4.36	3.03	5.58	5.45	2.77	2.92
Tm	0.74	0.64	0.86	0.66	0.33	0.87	0.66	0.45	0.81	0.81	0.39	0.43
Yb	4.77	4.14	5.69	4.29	2.18	5.77	4.21	2.87	5.38	5.33	2.52	2.86
Lu	0.73	0.62	0.86	0.64	0.33	0.85	0.65	0.44	0.81	0.80	0.37	0.43
Hf	4.00	3.14	4.44	3.43	1.29	4.61	3.18	1.67	4.31	4.12	2.16	1.60
Ta	0.26	0.19	0.29	0.32	0.08	0.31	0.20	0.06	0.27	0.27	0.23	0.06
W	n.d.	n.d.	n.d.	n.d.	n.d.	n.d.	n.d.	0.10	0.14	0.06	0.13	0.03
Pb	0.57	0.45	1.03	0.19	0.11	0.19	2.34	0.35	0.47	0.54	0.18	0.41
Bi	n.d.	n.d.	n.d.	n.d.	n.d.	n.d.	n.d.	0.01	0.01	0.01	0.01	0.01
Th	0.29	0.23	0.42	0.32	0.14	0.35	0.27	0.24	0.31	0.31	0.66	0.20
U	0.17	0.12	0.23	0.16	0.17	0.21	0.14	0.19	0.91	0.33	0.40	0.09

$Fe_2O_3^* = $ total Fe as Fe_2O_3.
n.d. = not determined; b.d. = below detection.
AC = accretionary complex; HP = high-P/T metamorphic complex; OP = ophiolitic complex.
[a] The data of major element compositions from Ota et al. (2007).
[b] Trace element compositions were determined using the solution of rock powder. Others were using solution of fused glass disks.

3.3. The ophiolitic complex

The ophiolitic complex is juxtaposed between the island arc complex and high P/T metamorphic complex (Fig. A2 online). The ophiolitic complex in the southern Gorny Altai consists of peridotites, amphibolite (metagabbro?), gabbroic lenses, non-sheeted dykes of basalt, gabbro and pyroxenite, massive and pillowed basaltic lavas and micritic limestones. The lithological assemblage in northern Gorny

99KR218[b]	98KR48	98KR50	KR71[a,b]	99CU4[b]	99CU182[b]	99CU23[b]	01CU12[b]	98CU41[b]	UZ12[b]	CU21	CU53[a,b]
W. Kurai	SW.Kurai	SW.Kurai	SW.Kurai	Chagan-Uzun	Chagan-Uzun	Chagan-Uzun	Chagan-Uzun	Chagan-Uzun	Chagan-Uzun	Chagan-Uzun	Chagan-Uzun
AC	AC	AC	HP	AC	AC	HP	HP	HP	OP	OP	OP
Dolerite	Basalt	Basalt	Basalt	Basalt	Basalt	Basalt	Basalt	Amphibolite	Basalt	Amphibolite	Amphibolite
3	3	3	1	3	1	2	3	4	1	2	1
47.43	47.06	49.39	47.57	52.09	49.53	47.18	45.00	46.82	51.44	49.37	49.00
1.82	2.21	2.68	1.15	2.23	0.82	2.31	2.88	1.06	1.65	0.82	2.13
12.13	12.05	14.11	14.11	16.33	14.26	13.60	14.16	14.19	13.28	13.99	14.66
10.92	13.34	10.21	10.26	9.72	12.23	15.18	14.03	10.47	12.58	13.11	14.34
0.17	0.18	0.14	0.18	0.11	0.18	0.23	0.21	0.17	0.31	0.20	0.22
8.01	10.48	7.93	7.09	2.79	6.72	4.79	6.63	10.30	3.92	5.64	6.70
12.88	7.98	6.12	12.82	3.93	6.55	7.01	8.90	7.87	6.76	9.72	8.20
2.37	2.21	3.55	3.24	5.14	4.13	3.05	2.47	3.10	3.99	3.31	4.09
0.38	0.13	0.14	0.07	0.58	0.17	0.56	0.42	0.84	0.02	0.56	0.26
0.15	0.16	0.19	0.10	0.26	0.06	0.17	0.23	0.23	0.06	0.04	0.22
2.39	3.14	4.82	3.66	5.64	4.00	3.85	3.61	2.93	4.52	1.10	2.05
98.64	98.93	99.28	100.26	98.82	98.65	97.90	98.53	97.98	98.53	97.84	101.89
875	764	881	461	958	427	946	1096	1313	473	336	990
66.6	33.0	31.6	40.4	32.4	38.4	44.8	38.4	32.3	38.0	43.8	48.2
347	319	329	260	278	257	452	380	268	451	406	478
125	509	708	333	354	156	34	54	573	23	37	129
40.0	52.3	50.8	53.2	35.4	42.4	44.1	50.2	44.7	32.3	39.1	52.5
46.7	254.1	262.7	49.2	133.8	91.6	21.8	80.8	227.8	15.0	27.1	53.8
153.1	111.4	137.8	87.3	12.2	102.3	53.6	142.0	64.9	64.4	94.3	83.9
66	100	95	66	68	76	119	125	79	75	94	129
16	17	16	16	20	12	20	22	16	16	15	19
1.4	1.6	1.3	1.2	1.2	1.6	1.9	1.9	1.6	1.6	1.4	1.5
0.3	0.4	2.5	0.4	0.3	0.2	1.3	1.8	22.1	1.1	0.3	0.5
0.07	0.29	0.32	0.06	0.05	0.05	0.10	0.09	0.06	0.06	b.d.	0.09
4.7	2.7	3.4	1.4	23.3	3.4	9.8	5.2	14.2	1.4	9.4	4.1
553	243	260	193	100	283	736	156	494	382	383	166
25.4	23.5	25.1	23.8	23.6	20.7	45.3	32.1	23.0	25.0	16.9	40.4
110	123	127	42	152	36	131	157	92	47	32	64
9.53	11.51	13.79	1.12	8.97	1.29	2.79	16.35	4.50	1.07	0.68	2.46
0.26	0.42	0.43	0.18	0.35	0.19	0.38	1.84	0.44	0.68	0.49	0.37
0.72	1.19	1.36	0.37	0.64	0.25	0.88	1.10	0.96	0.42	0.40	0.37
0.01	0.04	0.14	0.16	0.53	0.09	0.44	0.24	7.64	1.01	0.05	2.81
0.19	0.49	0.74	0.04	9.18	0.24	0.91	3.17	1.42	1.62	0.40	0.20
127	190	184	44	42	185	428	298	326	165	113	61
8.58	8.30	8.11	2.30	8.16	1.44	6.38	15.25	19.47	2.06	1.82	3.56
21.31	21.86	22.99	7.35	20.35	4.25	18.74	35.81	45.20	6.37	4.91	11.86
3.06	3.21	3.41	1.26	2.76	0.76	3.05	4.85	5.91	1.09	0.76	2.07
14.98	15.83	16.60	7.10	13.09	4.42	16.51	22.69	25.98	6.32	4.12	11.81
4.31	4.55	4.70	2.49	3.50	1.71	5.34	5.92	5.59	2.36	1.40	4.37
1.39	1.48	1.60	0.91	1.02	0.57	1.71	2.14	1.57	0.84	0.62	1.56
4.67	5.02	5.09	3.01	3.73	2.31	6.37	6.27	5.12	3.08	1.98	5.28
0.84	0.85	0.85	0.61	0.67	0.49	1.27	1.08	0.78	0.64	0.40	1.11
4.93	4.69	4.77	3.99	4.14	3.42	8.15	6.15	4.27	4.19	2.58	7.27
0.99	0.91	0.93	0.87	0.91	0.77	1.76	1.21	0.85	0.93	0.60	1.59
2.64	2.30	2.36	2.39	2.70	2.30	5.03	3.18	2.35	2.70	1.73	4.46
0.36	0.31	0.31	0.36	0.40	0.35	0.73	0.43	0.33	0.40	0.27	0.65
2.24	1.89	1.86	2.26	2.64	2.33	4.92	2.67	2.13	2.60	1.80	4.13
0.33	0.28	0.27	0.32	0.40	0.36	0.74	0.38	0.32	0.39	0.29	0.61
2.90	3.18	3.44	1.08	3.73	1.08	3.60	4.13	2.43	1.34	1.01	1.71
0.65	0.78	0.98	0.13	0.59	0.10	0.21	1.16	0.28	0.09	0.05	0.22
0.06	0.10	0.26	n.d.	0.11	0.07	0.07	2.15	0.23	0.09	0.03	n.d.
0.16	1.06	1.77	0.61	1.56	0.21	0.77	0.51	6.12	0.34	1.19	0.20
0.00	0.01	0.01	n.d.	0.01	0.01	0.01	0.01	0.01	0.01	0.01	n.d.
0.74	0.66	0.77	0.07	1.15	0.08	0.48	1.21	2.33	0.14	0.25	0.17
0.18	0.23	0.51	0.04	0.50	0.02	0.30	0.43	0.46	0.15	0.23	0.91

Altai is somewhat different and composed of layered gabbros and pyroxenites, sheeted dykes, pillow lavas and volcanic breccia, and siliceous and argillaceous sedimentary rocks. The complex underwent low-pressure metamorphism, from prehnite–pumpellyite to amphibolite facies (Ota et al., 2007). Some dykes intruding peridotites are geochemically similar to rocks of the calc–alkaline island arc series (Buslov et al., 1993, 2002), and are less metamorphosed than their host rock.

4. Sample description

4.1. The accretionary complex

The sample localities are shown in Figs. 4 and A1–A4 online. Porphyritic basalts and dolerites were selected from the accretionary complex for geochemical and isotopic analyses. Basaltic samples are hypocrystalline to holocrystalline and have phenocryst assemblages of clinopyroxene + plagioclase, clinopyroxene, and plagioclase. Coarser grained samples show sub-ophitic textures. The plagioclase phenocrysts are prismatic or tabular and some show alteration to albite or chlorite. The groundmass has intersertal or intergranular texture and

Table 2
Major and trace element compositions of greenstones from Northern Gorny Altai.

Sample	U45	U48[a]	U49	U51[a]	U52	AT12[a]	AT41[a]	AT48	AT49[a]	AT74[a]	AT76
Area	Ust-Syoma	Ust-Syoma	Ust-Syoma	Ust-Syoma	Ust-Syoma	Teletskoy	Gorno-Altaisk	Gorno-Altaisk	Gorno-Altaisk	Gorno-Altaisk	Gorno-Altaisk
Complex	AC	AC	AC	AC	AC	OP	AC	AC	AC	AC	AC
Vithology	Basalt	Basalt	Basalt	Basalt	Basalt	Basalt	Basalt	Basalt	Basalt	Dolerite	Basalt
Group	3	3	3	3	3	3	2	3	3	2	2
(wt.%)											
SiO$_2$	47.86	47.20	46.29	47.74	47.56	51.06	48.36	45.06	44.35	44.80	44.51
TiO$_2$	1.89	2.13	2.25	2.34	2.40	1.43	0.78	2.76	3.68	1.49	1.61
Al$_2$O$_3$	13.23	13.06	13.78	13.78	13.49	18.21	15.11	18.38	13.64	13.46	14.30
Fe$_2$O$_3$*	12.83	14.74	15.44	14.05	14.64	7.37	10.94	12.92	17.30	14.66	13.82
MnO	0.14	0.17	0.15	0.16	0.14	0.09	0.24	0.16	0.24	0.19	0.16
MgO	6.76	5.92	8.04	7.82	7.34	4.14	7.72	3.72	5.12	6.86	6.44
CaO	10.93	9.11	7.38	6.99	6.82	6.78	8.49	7.15	7.84	11.84	12.59
Na$_2$O	2.45	3.74	2.83	3.59	3.62	5.10	2.40	4.22	3.83	1.81	1.69
K$_2$O	0.43	0.09	0.26	0.13	0.10	0.40	2.07	0.39	0.03	0.14	0.03
P$_2$O$_5$	0.15	0.12	0.15	0.18	0.21	0.20	0.22	0.32	0.41	0.07	0.08
LOI	2.55	3.73	3.15	2.91	2.95	3.20	1.09	3.00	2.38	2.92	3.46
Total	99.22	100.01	99.71	99.67	99.26	97.98	97.41	98.07	98.81	98.23	98.69
(ppm)											
P	573	562	639	815	834	1031	1024	1688	1788	465	332
Sc	36.2	27.4	35.6	29.9	32.6	30.2	35.7	27.8	26.0	39.4	40.8
V	382	214	416	279	381	246	246	254	305	595	643
Cr	354	34	184	24	41	160	177	19	34	31	17
Co	47.8	45.6	56.6	47.9	48.4	24.8	37.9	36.7	50.8	50.4	40.8
Ni	134.9	65.1	111.0	74.8	76.4	75.4	47.6	23.6	42.3	45.6	34.6
Cu	50.7	156.9	192.6	144.8	122.3	48.5	232.7	109.4	49.8	169.9	128.2
Zn	88	95	127	113	110	50	117	107	131	70	51
Ga	17	20	21	20	19	15	14	23	23	16	14
Ge	1.8	2	1.7	1.6	1.6	1.0	1.3	1.4	2.1	1.8	1.3
As	0.4	0.5	0.3	0.5	0.3	0.5	2.3	0.4	0.6	0.2	0.0
Se	0.27	0.06	0.30	0.06	0.29	0.06	0.04	0.01	0.07	0.07	b.d.
Rb	8.2	2.7	5.0	2.8	2.4	5.0	55.5	3.4	1.6	7.1	1.4
Sr	342	190	320	334	281	320	295	1815	312	536	137
Y	22.3	21.1	23.1	24.2	26.5	25.4	14.9	21.6	25.4	20.9	19.9
Zr	110	120	131	127	129	81	46	165	191	53	48
Nb	13.85	15.56	16.73	16.06	17.03	10.82	2.86	23.48	26.46	1.59	1.38
Mo	0.70	0.64	2.01	0.54	1.05	0.23	0.28	0.77	0.50	0.30	0.07
Sn	1.20	1.42	1.36	1.43	1.46	1.24	0.74	1.75	1.89	0.57	0.47
Sb	0.08	0.24	0.06	0.14	0.05	0.19	1.89	0.05	0.07	1.03	0.06
Cs	0.14	0.43	0.21	0.48	0.42	0.04	4.56	0.30	0.42	1.95	0.43
Ba	57	40	47	59	28	144	401	1691	149	69	1
La	10.82	9.88	12.58	11.69	12.32	12.78	4.98	16.75	22.72	3.71	2.83
Ce	25.98	24.48	29.88	28.33	30.31	27.79	11.63	38.29	52.51	9.60	7.43
Pr	3.52	3.12	4.03	3.82	4.13	3.67	1.62	4.91	6.77	1.45	1.12
Nd	16.12	14.47	18.50	17.65	19.09	16.63	7.72	21.98	29.99	7.58	5.89
Sm	4.28	3.87	4.80	4.56	4.90	4.22	2.18	4.95	6.91	2.41	1.88
Eu	1.53	1.32	1.78	1.48	1.61	1.42	0.73	2.13	2.23	0.87	0.66
Gd	4.60	4.05	5.06	4.74	5.24	4.45	2.39	5.24	6.66	2.89	2.47
Tb	0.78	0.71	0.84	0.82	0.88	0.76	0.43	0.81	1.03	0.56	0.48
Dy	4.33	4.03	4.73	4.60	4.97	4.41	2.58	4.15	5.33	3.59	3.04
Ho	0.86	0.78	0.92	0.89	0.98	0.89	0.54	0.78	0.98	0.77	0.67
Er	2.23	2.02	2.37	2.30	2.56	2.41	1.53	1.96	2.45	2.18	1.88
Tm	0.30	0.27	0.33	0.31	0.34	0.32	0.22	0.25	0.32	0.32	0.28
Yb	1.83	1.67	1.96	1.92	2.08	2.03	1.49	1.57	1.92	2.11	1.83
Lu	0.27	0.24	0.30	0.28	0.31	0.29	0.22	0.22	0.28	0.32	0.28
Hf	2.92	3.02	3.45	3.26	3.33	2.00	1.17	3.89	4.77	1.44	1.33
Ta	0.90	1.06	1.11	1.15	1.13	0.82	0.19	1.48	1.86	0.11	0.08
W	0.22	0.08	0.20	0.12	0.18	0.24	0.59	0.15	0.18	0.05	0.11
Pb	1.75	1.70	2.61	1.43	2.02	2.77	10.93	1.71	0.53	0.31	1.04
Bi	0.00	0.00	0.00	0.00	0.01	0.00	0.00	0.01	0.00	0.01	0.01
Th	0.86	1.00	1.08	1.09	1.06	1.11	0.79	1.70	1.99	0.31	0.31
U	0.16	0.10	0.19	0.24	0.33	0.38	0.51	0.50	0.54	0.13	0.13

Fe$_2$O$_3$* = total Fe as Fe$_2$O$_3$.
b.d. = below detection.
AC = accretionary complex; OP = ophiolitic complex.
  [a] Trace element compositions were determined by using the solution of rock powder. Others were by using solution of fused glass disks.

is composed of plagioclase, clinopyroxene, magnetite and devitrified glass. The dolerites show ophitic or equigranular texture with albitic plagioclase, clinopyroxene and magnetite.

All mafic rocks from the accretionary complex have undergone alteration and metamorphism. Chlorite, albite, prehnite, pumpellyite, calcite and opaque minerals are the common secondary minerals. Amphiboles are present in the dolerite samples, but absent in the basalts.

4.2. The high-P/T metamorphic complex

In the present study, only slightly metamorphosed and less deformed mafic schists and amphibolite were chosen for chemical and isotopic analyses. No eclogites were analyzed. The moderately deformed mafic schists are porphyritic and hypocrystalline and have clinopyroxene and plagioclase phenocryst with secondary chlorite, calcite and opaque minerals. Occasionally prehnite, pumpellyite, actinolite, and hornblende are observed.

4.3. The ophiolitic complex

Basalts and amphibolites were selected from the ophiolitic complex. The basalts have texture and mineralogy similar to that of mafic rocks from the accretionary complex. The amphibolites show fine to coarse-grained granular texture and are massive to moderately foliated. A few fibrous amphibolites also occur. The major mineral assemblage is amphibole, plagioclase and Fe–Ti oxide. Quartz, carbonate minerals, titanite, chlorite and epidote are common accessory phases. There are a few relict clinopyroxene crystals. Amphibole is fine to coarse-grained, acicular to granular and exhibits various pleochroism; greenish yellow to green, yellowish brown to green, and pale brown to brown. Plagioclase is fine-grained granular to coarse-grained tabular.

5. Analytical procedures

Samples were crushed using a steel jaw crusher and then powdered in an agate mill. Major element compositions were determined by X-ray fluorescence (XRF) techniques on fused glass beads using a Rigaku RIX-2000 spectrometer at the Department of Geosciences, National Taiwan University. The analytical uncertainties are better than 5% for all elements (Lee et al., 1997).

Trace elements were measured on solutions of fused glass beads or powdered samples using an inductively coupled plasma-mass spectrometer (ICP-MS, Agilent 7500s) also at the Department of Geosciences, National Taiwan University. Fused glass beads were dissolved using a HF–HNO$_3$ (2:1) mixture in screw-top Teflon beakers for >2 h at ~100 °C, followed by evaporation to dryness, and then dissolved using 1:2 HNO$_3$ for a night at ~100 °C. This procedure was followed by evaporation to dryness and dissolved in 2% HNO$_3$ before ICP-MS analysis. Powdered samples were dissolved using a HF–HNO$_3$ (2:1) mixture in screw-top Teflon beakers for 2 days at ~100 °C. This procedure was followed by evaporation to dryness, refluxing in 6N HCl and drying twice, and then dissolution in 1N HCl. The procedure was repeated until the complete dissolution. The final solution was evaporated to dryness, then refluxed in 6N HNO$_3$ and dried three times, and dissolved in 2% HNO$_3$ before ICP-MS analysis. The ICP-MS analytical procedure has been described by Yang et al. (2005). The analytical errors are better than 5%.

Sr and Nd isotope ratios were measured using a Finnigan MAT 262 or a TRITON mass spectrometer at the Institute of Earth Sciences, Academia Sinica. Chemical separation was carried out using the conventional ion exchange techniques. Sr and Nd isotopic ratios were corrected by normalizing to $^{86}Sr/^{88}Sr = 0.1194$ and $^{146}Nd/^{144}Nd = 0.7219$. Analyses of the NBS 987 Sr and JMC Nd standard throughout the period of analysis yielded $^{86}Sr/^{87}Sr$ values of 0.710238 ± 0.000016 (2σ) and $^{143}Nd/^{144}Nd$

of 0.511812 ± 0.000007 (2σ), respectively. Procedural blanks were approximately 330 pg Sr and 300 pg Nd. Within-run precision, expressed as 2σ_m, for Sr and Nd is better than 0.000016 and 0.000010, respectively.

6. Geochemistry

Representative geochemical analyses for the Gorny Altai greenstones are shown in Tables 1 and 2 (complete data for the southern Gorny Altai is available online (Table A1)). In a Zr/TiO$_2$ vs. Nb/Y plot (Fig. 5a), the Gorny Altai greenstones fall in the subalkaline basalt field or near the boundary between alkaline and subalkaline basalt fields. In a SiO$_2$ vs. FeO*/MgO plot (Fig. 5b), the southern and northern Gorny Altai greenstones fall in the tholeiitic field. The basaltic rocks of the accretionary, high-P/T metamorphic and ophiolitic complexes show no difference.

Chondrite-normalized rare earth element (REE) patterns for the Gorny Altai greenstones are shown in Fig. 6. Greenstones from the accretionary complex have REE patterns varying from light (L) REE-depleted and flat heavy (H) REE to LREE-enriched and HREE-depleted (Fig. 6a). REE patterns of greenstones from the high-P/T metamorphic complexes have similar patterns as those from the accretionary complex (Fig. 6b). Greenstones from the ophiolitic complex show LREE-depleted to flat patterns (Fig. 6c). Greenstones from the northern Gorny Altai have flat and LREE-enriched and HREE-depleted patterns (Fig. 6d).

Y vs. Nb plot for the Gorny Altai greenstones is shown as Fig. 7 which shows that greenstones from the southern Gorny Altai have
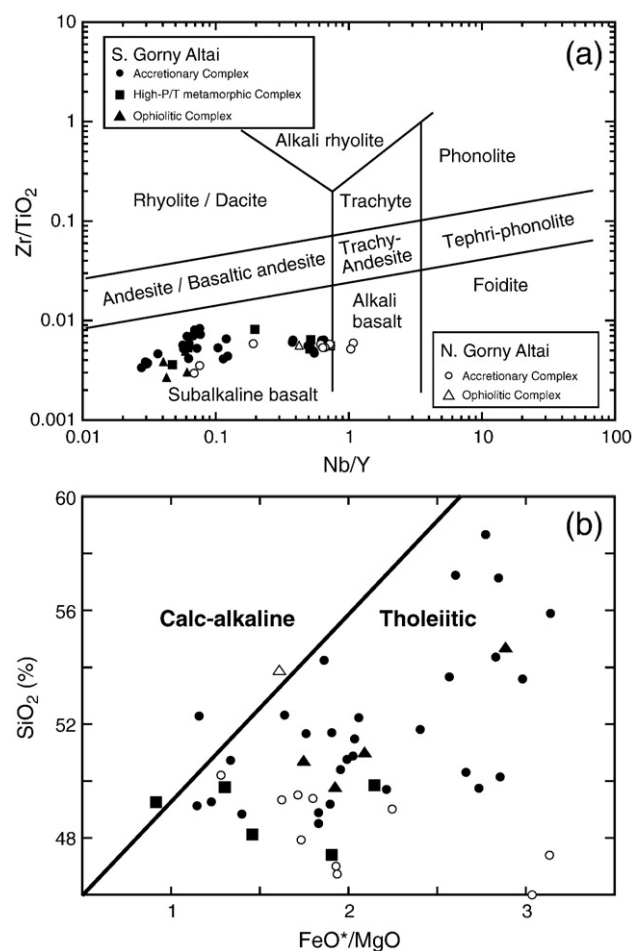
Fig. 5. (a) Zr/TiO$_2$ vs. Nb/Y and (b) SiO$_2$ vs. FeO*/MgO plots. The classification of (a) is referred to Pearce (1996). The division line between calc–alkaline and tholeiite of (b) is from Miyashiro (1973).
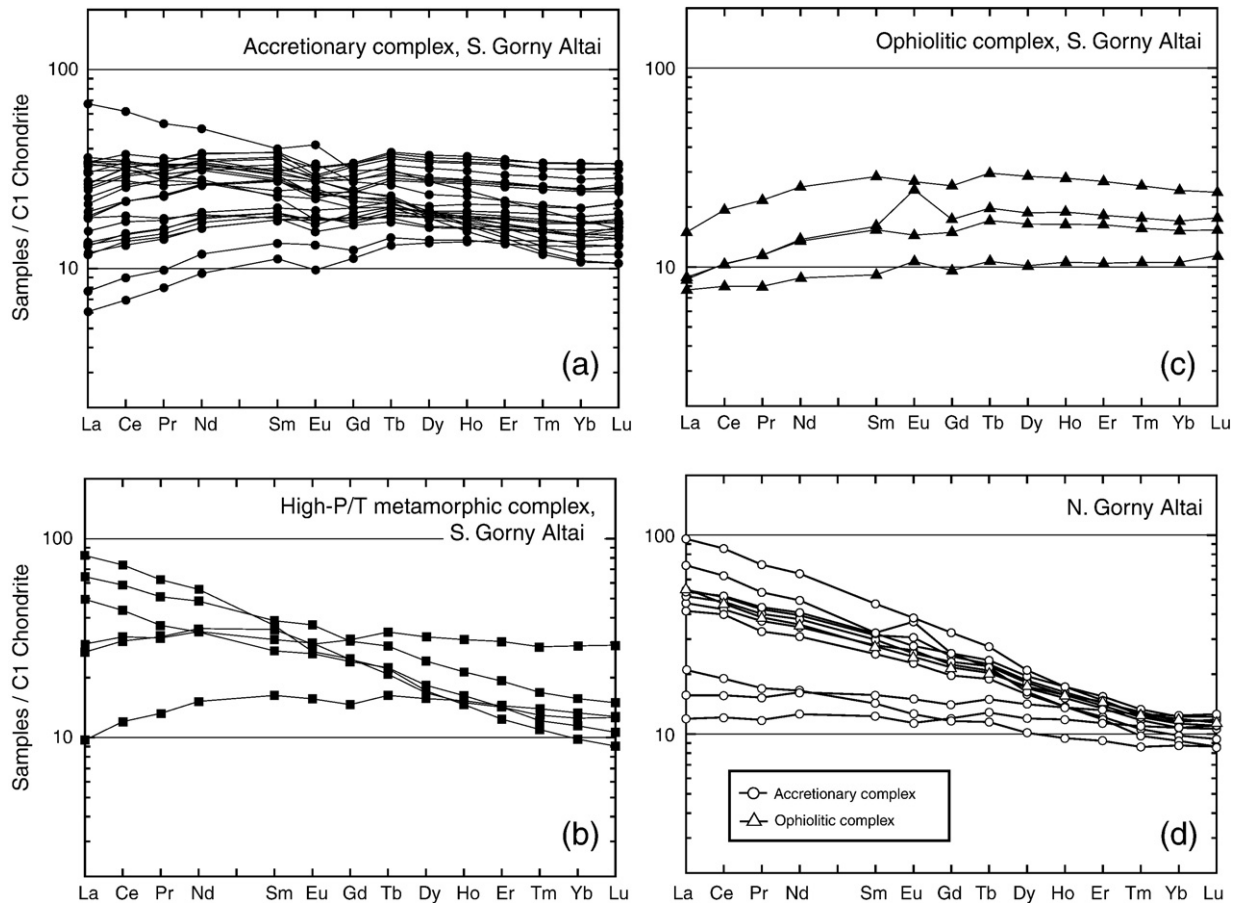
Fig. 6. Chondrite-normalized REE patterns for the samples from (a) the accretionary complex, (b) the high P/T complex and (c) the ophiolitic complex in southern Gorny Altai and samples from (d) northern Gorny Altai. The values of C1 chondrite are from Sun and McDonough (1989).

two trends: a steep trend corresponding to a low Nb/Y ratio and a shallow trend corresponding to a high Nb/Y ratio. On the other hand, greenstones from the northern Gorny Altai only show the shallower trend. The variation suggests that these greenstones did not form by one episode of partial melting and/or from the same mantle source.

The Sr–Nd isotopic results are given in Table 3. The $\varepsilon_{Nd}(t)$ values are calculated assuming an eruption age of ~600 Ma which is based on the deposition age of the limestone cap (Uchio et al., 2004). All greenstone samples have positive $\varepsilon_{Nd}(600\ Ma)$ values (+4 to +9).

Fig. 7. Y vs. Nb plot showing two trends: (1) a steep trend and (2) a near-horizontal trend.

The Gorny Altai greenstones have variable $I_{Sr}(600\ Ma)$ values form (0.7035 to 0.7075; Fig. 8) indicating possible Sr mobilization during seawater alteration (see Section 7.1). The range of $\varepsilon_{Nd}(600\ Ma)$ values suggests that the Gorny Altai greenstones were probably derived from an isotopically heterogeneous source.

7. Discussion

7.1. Effect of alteration and metamorphism

The ubiquitous presence of secondary minerals and high loss on ignition (LOI) contents (1–6 wt.%) indicates that the Gorny Altai greenstones may have undergone a significant secondary alteration and a modification of their chemical compositions. It is clear that some elements have been mobilized based on their incoherent behavior in primitive mantle normalized multi-element plots (not shown). Elements such as Sb, Cs, Pb, Rb, Ba, K, U, and P are known to be mobile during seawater alteration (e.g., Jochum and Verma, 1996; Alt and Honnorez, 1984; Bach et al., 2001). The Sr–Nd diagram shows a subhorizontal trend off of the oceanic basalt array (Fig. 8). This could be caused by the isotopic exchange with the seawater Sr as demonstrated for Cretaceous MORB of deep-sea drilling (Jahn et al., 1980). Consequently, the following discussion will focus on the abundances and ratios of immobile elements and Nd isotope compositions.

7.2. Chemical classification of greenstones

Based on these geochemical characteristics, the Gorny Altai greenstones are unlikely to have been formed from a single source.

Table 3
Sr and Nd isotopic compositions of greenstones from Gorny Altai.

Sample	Area	Complex	Lithology	Group	Rb	Sr	$^{87}Rb/^{86}Sr$	$^{87}Sr/^{86}Sr$	$2\sigma_m$	$I_{Sr}(600)$	Sm	Nd	$^{147}Sm/^{144}Nd$	$^{143}Nd/^{144}Nd$	$2\sigma_m$	$\varepsilon_{Nd}(0)$	$\varepsilon_{Nd}(600)$
KR80	W.Kurai	AC	Basalt	1	7.37	292*	0.073	0.705930	9	0.70592	5.08*	14.9*	0.2056	0.513074	10	8.5	7.8
KR81	W.Kurai	AC	Basalt	1	6.34	240*	0.076	0.705701	14	0.70569	4.19*	12.2*	0.2075	0.513098	5	9.0	8.1
KR82	W.Kurai	AC	Basalt	1	3.61	190*	0.055	0.705108	15	0.70510	5.90*	17.5*	0.2033	0.513071	7	8.4	7.9
KR83	W.Kurai	AC	Dolerite	1	10.7	132*	0.234	0.706391	13	0.70637	4.88*	14.6*	0.2013	0.513044	6	7.9	7.5
KR86	W.Kurai	AC	Basalt	2	0.44	84.4*	0.015	0.705471	10	0.70547	2.05*	5.52*	0.2244	0.513134	6	9.7	7.6
KR87	W.Kurai	AC	Basalt	1	4.63	354*	0.038	0.705158	12	0.70515	5.83*	17.8*	0.1984	0.513057	7	8.2	8.1
KR90	W.Kurai	AC	Basalt	1	1.94	255*	0.022	0.706480	10	0.70648	4.24*	12.4*	0.2061	0.513088	7	8.8	8.0
98KR177	W.Kurai	AC	Basalt	2	1.08	85.1	0.037	0.704820	11	0.70482	3.01	8.18	0.2222	0.513078	6	8.6	6.6
98KR269	W.Kurai	AC	Basalt	1	2.55	171.9	0.043	0.704851	14	0.70485	5.72	16.18	0.2139	0.513073	6	8.5	7.2
98KR400	W.Kurai	AC	Basalt	1	0.30	75.8	0.011	0.704347	15	0.70435	5.38	16.1*	0.2017	0.513074	5	8.5	8.1
99KR17	W.Kurai	AC	Basalt	4	6.02	301*	0.058	0.705591	13	0.70559	4.29	14.08	0.1841	0.512874	5	4.6	5.6
99KR68	W.Kurai	AC	Basalt	2	0.80	94*	0.025	0.705047	14	0.70504	2.72	7.23	0.2273	0.513097	6	9.0	6.6
99KR218	W.Kurai	AC	Dolerite	3	4.74	553*	0.025	0.705048	10	0.70505	4.29	14.32	0.1812	0.512797	7	3.1	4.3
KR16	SW.Kurai	AC	Basalt	3	9.10	218*	0.121	0.704830	13	0.70482	6.13*	23.6*	0.1574	0.512826	8	3.7	6.7
98KR48	SW.Kurai	AC	Basalt	3	2.77	245*	0.033	0.706310	9	0.70631	4.57	15.14	0.1823	0.512801	6	3.2	4.3
KR71	SW.Kurai	HP	Basalt	1	1.35	193*	0.020	0.703546	15	0.70354	2.49*	7.10*	0.2122	0.513144	8	9.9	8.7
99CU4	Chagan-Uzun	AC	Basalt	3	23.3	104.8	0.642	0.707637	13	0.70758	3.50*	12.61	0.1679	0.512823	7	3.6	5.8
99CU23	Chagan-Uzun	HP	Dolerite	2	9.81	776.4	0.037	0.706606	16	0.70660	5.29	15.44	0.2071	0.513035	6	7.8	7.0
01CU12	Chagan-Uzun	HP	Basalt	3	5.24	163.0	0.093	0.704649	10	0.70464	5.87	21.32	0.1664	0.512741	6	2.0	4.3
98CU41	Chagan-Uzun	HP	Amphibolite	4	14.2	506.2	0.081	0.704796	10	0.70479	5.41	26.0*	0.1260	0.512732	6	1.8	7.3
UZ12	Chagan-Uzun	OP	Basalt	1	1.43	396.2	0.010	0.706406	13	0.70641	2.33	6.32*	0.2225	0.513130	7	9.6	7.6
CU53	Chagan-Uzun	OP	Amphibolite	1	4.14	166*	0.072	0.705423	12	0.70542	4.37*	11.8*	0.2235	0.513164	8	10.3	8.2
U48	Ust-Syoma	AC	Basalt	3	2.72	194.7	0.040	0.704105	14	0.70410	4.03	14.45	0.1686	0.512756	6	2.3	4.5
U51	Ust-Syoma	AC	Basalt	3	2.82	349.9	0.023	0.704235	9	0.70423	4.73	17.45	0.1638	0.512743	6	2.0	4.6
AT12	Teletskoy	OP	Basalt	3	5.04	324.3	0.045	0.703841	8	0.70384	4.26	16.08	0.1603	0.512813	7	3.4	6.2
AT49	Gorno-Altaisk	AC	Basalt	3	1.57	337.5	0.013	0.703738	10	0.70374	7.13	29.42	0.1464	0.512661	7	0.5	4.3
AT74	Gorno-Altaisk	AC	Dolerite	2	7.06	583.1	0.035	0.703514	9	0.70351	2.49	7.47	0.2018	0.512976	7	6.6	6.2

AC = accretionary complex; HP = high-P/T metamorphic complex; OP = ophiolitic complex.
The depositional age of caped limestone is taken as the erupted age of basalt. The limestone age was determined by bulk Pb–Pb isochron method (Uchio et al., 2004).
All the concentrations of Rb and those of Sr, Sm and Nd with asterisks are obtained by ICP-MS. These errors are <6%, <3%, <2.5%, and <2.5% in RSD, respectively.
The concentrations of Sr, Sm, and Nd without asterisks are obtained by TIMS-ID.

In fact, four chemical groups can be distinguished (Fig. 9): (1) Group 1 rocks show depletion in highly incompatible elements (Th, Nb, Ta and La), without negative Nb–Ta anomaly, (2) Group 2 rocks have slight to no depletion in highly incompatible elements, with negative Nb–Ta anomaly, (3) Group 3 rocks are enriched in highly incompatible elements, without negative Nb–Ta anomaly, and (4) Group 4 rocks show variable enrichment in highly incompatible elements, with negative Nb–Ta anomalies. Despite the chemical distinctions, the petrographical features are rather similar between groups.

The accretionary and high-P/T metamorphic complexes in southern Gorny Altai contain all four groups of greenstones (Fig. 9a–e). The protoliths of greenstones from the high P/T metamorphic complex could be similar to the accretionary complexes. The ophiolitic complex

in southern Gorny Altai lacks Groups 3 and 4 (Fig. 9f). The northern Gorny Altai has only Groups 2 and 3 greenstones (Fig. 9g). However, because the greenstones from these complexes have both oceanic (with no negative Nb–Ta anomaly) and subduction-related (with a negative Nb–Ta anomaly) geochemical signatures, their petrogenesis is similar to that of the greenstones from the accretionary complex in southern Gorny Altai. For the ophiolite complex in northern Gorny Altai, there are fewer data available, but the greenstones were generated in the same setting as those from other complexes in Gorny Altai.

7.3. Comparison with modern typical volcanic sequences

All of the Gorny Altai greenstones are structurally associated with micritic limestones without terrigenous materials. This indicates that they formed in shallow water in an oceanic environment (Uchio et al., 2004). The basalts were not generated at a normal mid-ocean ridge, mature island arc or active continental margin, because MORB is typically overlain by thick chert deposits, whereas volcanic rocks of mature island arc and continental margin are usually associated with sediments including terrigenous materials. The petrography of the Gorny Altai greenstones shows that the parental magma went through an early clinopyroxene crystallization phase. It is markedly different from the typical MORB magmas which are mainly controlled by olivine and plagioclase fractionation.

Group 1 greenstones are depleted in highly incompatible elements, and are similar to those of normal (N-) MORB except that trace element abundances are generally higher (Fig. 9). In comparison, Group 2 greenstones are slightly depleted in highly incompatible elements or have flat primitive mantle normalized patterns with negative Nb–Ta anomalies; they resemble subduction-related volcanic rocks. Group 3 rocks are enriched in highly incompatible elements and are similar to OIB or enriched (E-) MORB. Group 4 greenstones are
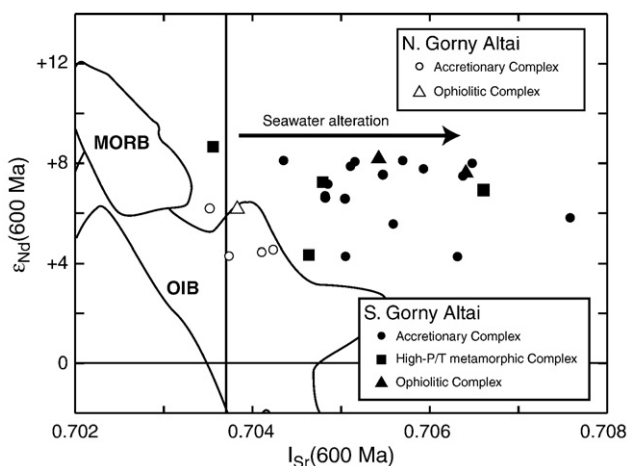
Fig. 8. ε_{Nd}(600 Ma) vs. I_{Sr}(600 Ma) diagram for the Gorny Altai greenstones. MORB and OIB fields at 600 Ma are modified from Zindler and Hart (1986).
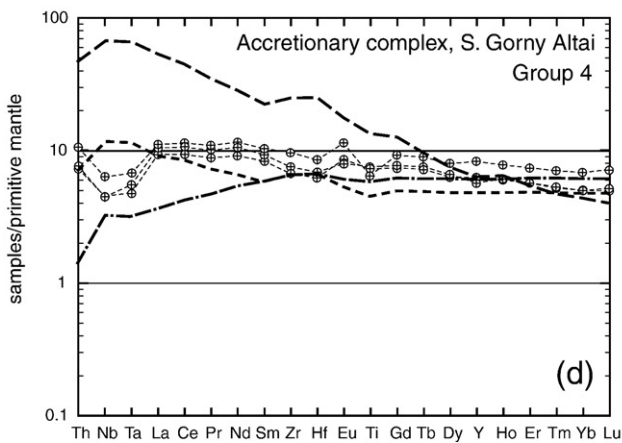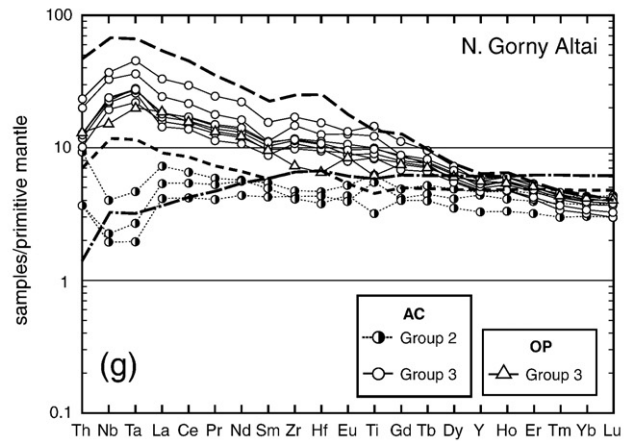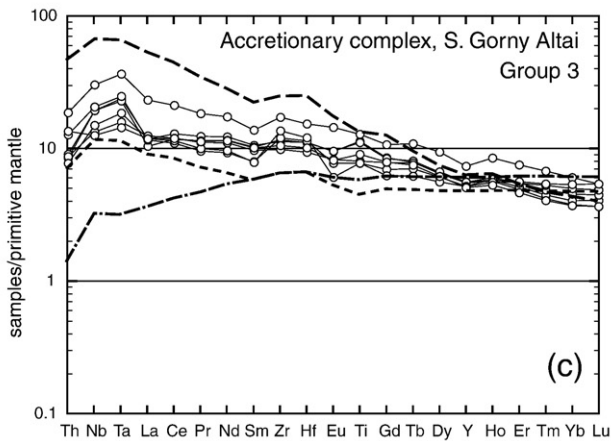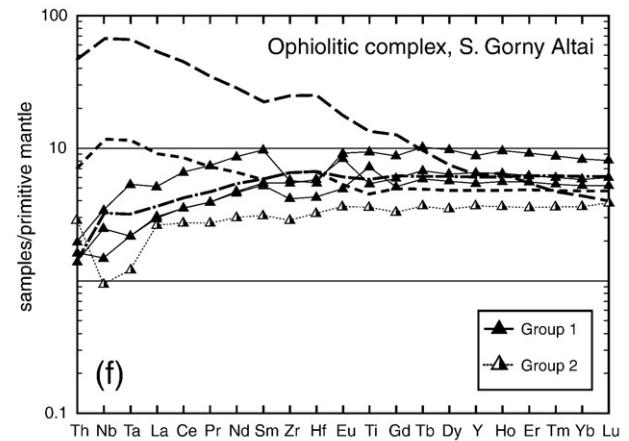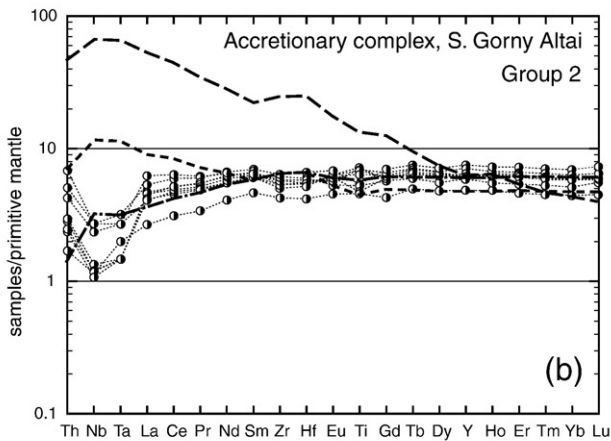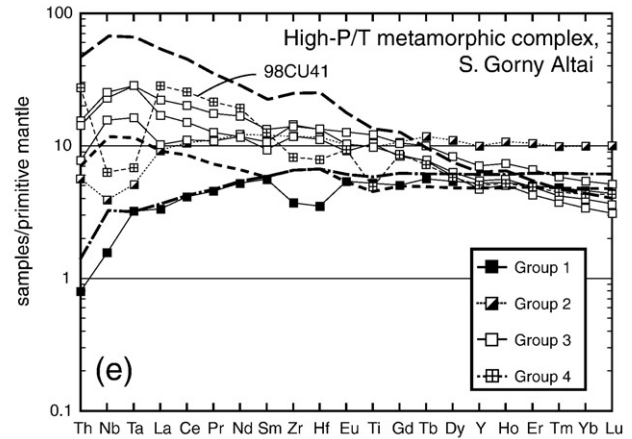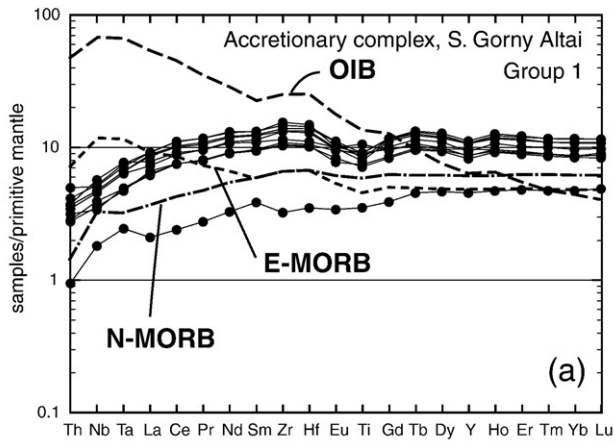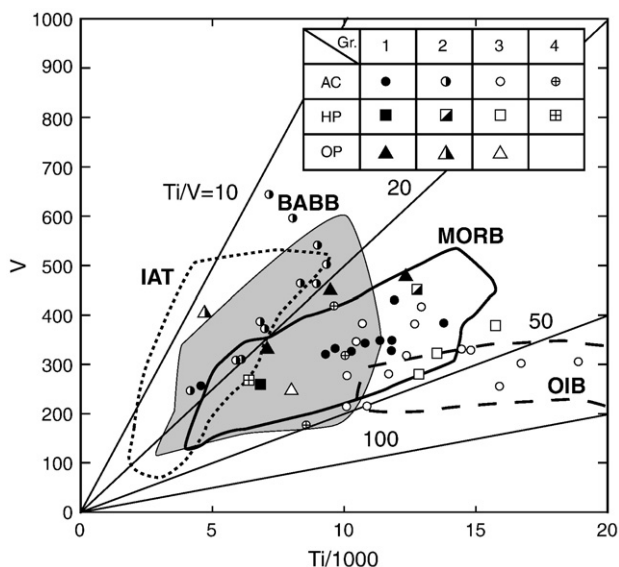
Fig. 10. V vs. Ti plot for the Gorny Altai greenstones. The fields of MORB, IAT, BABB and OIB are from Shervais (1982).
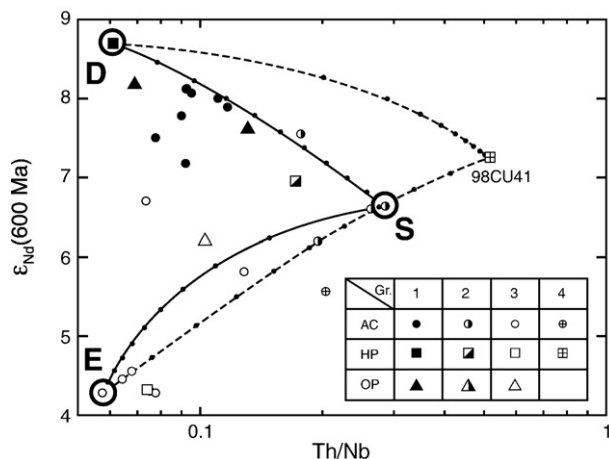
Fig. 11. ε_{Nd}(600 Ma) vs. Th/Nb diagram. The end-members of "D", "E" and "S" are explained in Section 7.4. Solid lines express the mixing between "S" and "D" or "E". Dashed lines express the mixing between 98CU41 (Group 4) and "D" or "E".

variably enriched in highly incompatible elements, and show a negative Nb–Ta anomaly; they resemble subduction-related volcanic rocks.

Group 1 greenstones fall in the MORB or back-arc-basin basalt (BABB) field on V vs. Ti plot (Fig. 10). Group 2 greenstones have lower Ti/V ratios than Group 1 and fall within the BABB or island arc tholeiite (IAT) fields. Ti/V ratios of Group 3 are higher than Group 1 and correspond to those of MORB or OIB. The distribution of Ti/V ratios for Group 4 overlaps with those of Group 1.

In summary, the trace element compositional signatures indicate that Group 1 is similar to N-MORB. However the geological and petrographical features point to a different tectonic setting than MORB, which is typically overlain by a thick chert deposit and contains mainly olivine and plagioclase phenocrysts. Groups 2 and 4 show subduction-related geochemical signatures, but the absence of associated terrigenous sedimentary rocks suggested that they were formed in proximity

of the continental margin or mature island arc. The generation of Group 3 rocks appears to have involved an enriched component like OIB or E-MORB. The chemical complexity and the apparent conflicting evidence for their tectonic settings will be discussed below.

7.4. Petrogenesis of the Gorny Altai greenstones

Although we divided the rocks into four chemical groups for descriptive purposes, each group does not form a distinct cluster in the ε_{Nd}(600 Ma) vs. Th/Nb diagram (Fig. 11) and the distribution of the data points can be explained by mixing between groups. The most depleted sample of Group 1 was regarded as end-member "D" and the most enriched sample of Group 3 was assumed as end-member "E". The sample having the largest Th/Nb ratio of Group 2 was regarded as the end-member of subduction-modified component ("S"). All but one of Group 4 (98CU41) fit the mixing line between the end-members "S" and "D" or "E". Although some of Groups 2–4 plot on or near the mixing line between 98CU41 and end-member "E", the trace element distribution patterns of Groups 2 and 4 that are depleted or only slightly enriched in highly incompatible elements could not be generated by mixing of 98CU41 and Group 3 that have enriched patterns (Fig. 9). Sample 98CU41 cannot be an end-member of mixing, but might be generated by a small degree of partial melting of a source more modified by subduction. In summary, the source of the Gorny Altai greenstones contains MORB-like depleted, OIB-like enriched, and subduction-modified components and all rocks are genetically related by the mixing of the components.

7.5. The tectonic setting of the Gorny Altai greenstones

7.5.1. Comparison with the modern oceanic island arc and back-arc-basin

The tectonic setting cannot be reliably inferred from a simple comparison of geochemical characteristics with modern volcanic sequences (e.g., Mullen, 1983; Pearce and Cann, 1973). The Gorny Altai greenstones have been proposed to be MORB and OIB (Dobretsov et al., 2004). Indeed, on the basis of geochemistry alone, Group 1 may be generated from a mid-ocean ridge. However, Group 1 lavas are overlain by limestone, unlike that of the typical MORB which is overlain by pelagic chert (Kanazawa et al., 2001). Moreover, clinopyroxene is predominant in the Gorny Altai lavas. This suggests that Group 1 lavas underwent crystal fractionation under different conditions from MORB. Group 1 from the accretionary complex of the Kurai area occurs in the same block as Group 2, which has a subduction geochemical signature (Fig. 4). Because the lavas both have oceanic and subduction-related signatures, they have to be formed in a tectonic setting which can explain the juxtaposition of both rock types.

The Philippine Sea Plate consists of oceanic island arcs, marginal basins and seamounts in a back-arc basin (e.g., Seno and Maruyama, 1984). During the initiation of subduction in the western Pacific, sea-floor spreading took place near the Pacific margin within the Western Philippine Basin and Celebes Sea. Geochemical features of the volcanic rocks from the Western Philippine Basin vary from N-MORB to OIB without a clear subduction component (e.g., Pearce et al., 1999). The earliest stages of subduction produced the protoarc, which is now mostly preserved in the Bonin and Mariana fore-arc. The volcanic rocks range from boninite to tholeiite in composition. Subsequently, a more typical arc (early arc) developed and is preserved along the Palau–Kyushu Ridge. A series of arc, arc-rifting and back-arc spreading events (recent arc) occurred along the Izu–Bonin–Mariana system. The volcanic rocks from the Palau–Kyushu Ridge and Izu–Bonin–

Fig. 9. Primitive mantle normalized multi-element plots for four groups of samples from the accretionary complex ((a)–(d)) in southern Gorny Altai and samples from (e) ophiolitic complex and (f) the high P/T complex in southern Gorny Altai and (g) northern Gorny Altai. Primitive mantle values and reference lines of N-MORB, E-MORB and OIB are from Sun and McDonough (1989).
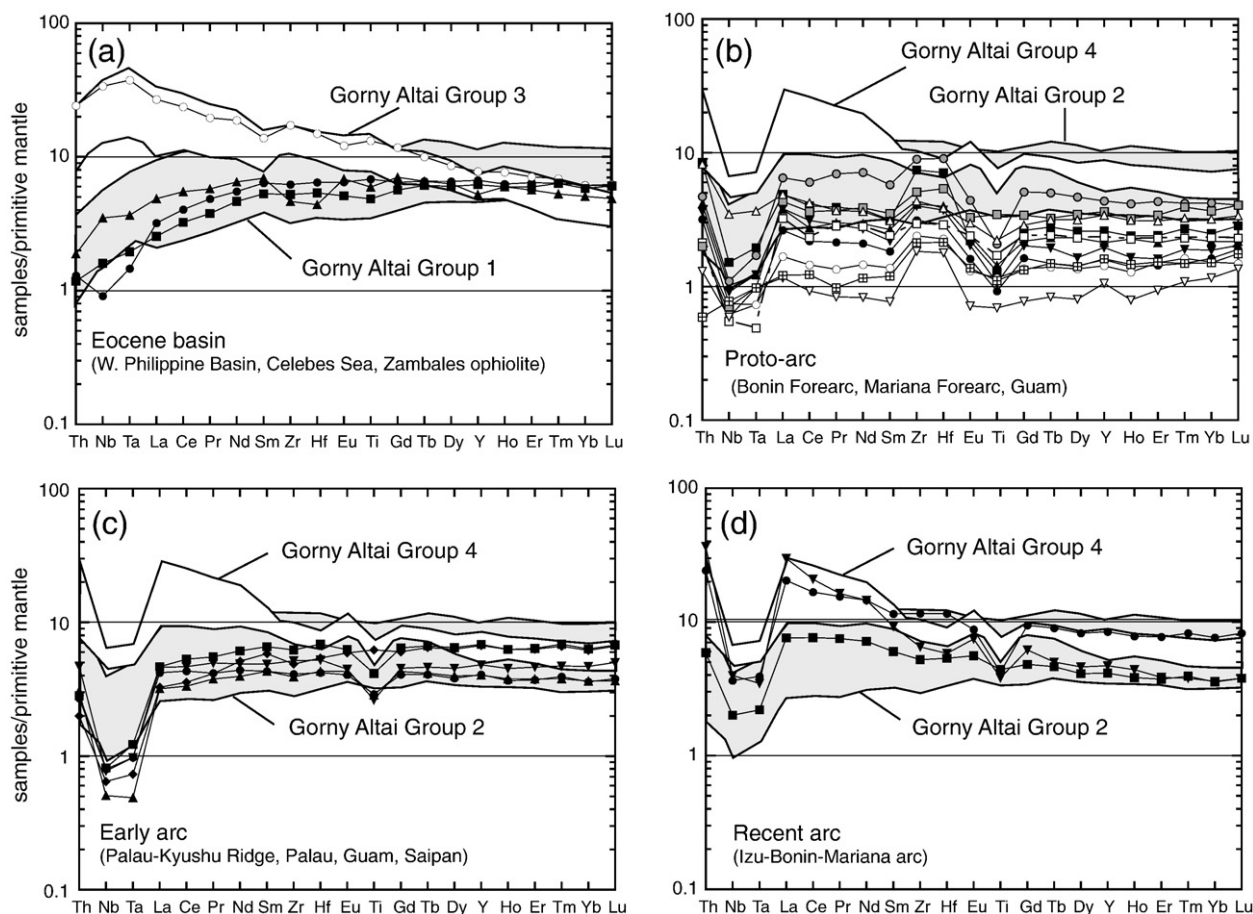
Fig. 12. Comparison of primitive mantle normalized multi-element plots between the Gorny Altai greenstones and the volcanic rocks of (a) Eocene basin, (b) Proto-arc, (c) Early arc and (d) Recent arc from the Western Pacific arc-basin systems. The fields show the range of the Gorny Altai greenstones. The data set of volcanic rocks from the Western Pacific arc-basin systems is from Pearce et al. (1999).

Mariana system (early and recent arc) range from tholeiitic to calc–alkaline and have flat to LREE-enriched REE patterns and negative Nb–Ta anomaly. The geochemical features of the Gorny Altai greenstones are similar to that of volcanic rocks distributed within the Philippine Sea Plate. Groups 1 and 3 correspond to compositions from the Eocene basin (Fig. 12a). Groups 2 and 4 correspond to the early and recent arc (Fig. 12c and d). However, the Gorny Altai greenstones are covered by micritic limestone or thin volcanic clastic deposit, whereas volcanic sequences from the Philippine Sea Plate are overlain by thick volcaniclastics derived from a successive volcanic activity (Salisbury et al., 2002).

7.5.2. Comparison with the Phanerozoic ophiolites

Some ophiolites, such as the Gorny Altai greenstones possess variable geochemical characteristics representing MORB, OIB and subduction settings. In the Coast Range ophiolite of California, dykes of MORB composition intrude older calc–alkaline plutons or volcanic sequences (Shervais et al., 2004). Lava flows of MORB or OIB composition overlie older subduction-related igneous suites and are intercalated with arc-like lavas. Elsewhere, volcanic rocks of the Kudi ophiolite in West Kunlun are sequentially characterized upward by geochemical features of N-MORB, E-MORB, IAB, BABB and boninite (Yuan et al., 2005).

The geochemical variation of these ophiolites may represent the temporal evolution of island arcs (Shervais, 2001; Yuan et al., 2005). The initiation of subduction within an oceanic region could lead to volcanism of MORB-like geochemical characteristics. As subduction develops, the underlying mantle wedge will be metasomatized by fluid released from subducting slab and thus the resulting magmas

have subduction signatures. This model may explain why there is a diverse range of magmas within the Kudi ophiolite and why there is a compositional evolution from MORB to boninite over time (Yuan et al., 2005). When an oceanic ridge is subducted, the subducted ridge continues to general asthenospheric melts (Shervais, 2001). In this case, magmas without subduction signatures may occur even after island arc has matured. The model can explain the geochemical variation of the Coast Range ophiolite and that dykes and lavas of MORB compositions may intrude and overlie the subduction-related magmas (Shervais, 2001).

The Gorny Altai greenstones are compositionally similar to the Coast Range and Kudi ophiolites. However, the Coast Range and Kudi ophiolites are associated with turbidites (Shervais et al., 2004; Yuan et al., 2005), whereas the Gorny Altai greenstones are overlain by micritic limestone.

7.5.3. Comparison with the Archean greenstone belt

Some Archean greenstone belts in the Superior Province, North America, comprise oceanic tholeiites, OIB-like basalts, subduction-influenced MORB-like rocks and mature calc–alkaline arc volcanic rocks (e.g., Hollings et al., 2000; Hollings and Wyman, 1999). Several models have been provided to explain the diverse geochemical features: (1) the complex nature of volcanism in the Meen–Dempster greenstone belt was interpreted to represent arc and back-arc development (Hollings et al., 2000), (2) the Abitibi greenstone belt was considered as formation of an arc above an accreted oceanic plateau (Desrochers et al., 1993), and (3) the coeval eruption of the diverse magma suites in the Lumby Lake greenstone belt is interpreted as the result of the sporadic subduction of plume-

influenced oceanic spreading centers and the eventual impingement of a mantle plume upon an active subduction zone (Hollings and Wyman, 1999).

The Gorny Altai greenstones are compositionally similar to these Archean greenstones in the Superior Province, but none of the above models can be used to explain the geological features of the Gorny Altai greenstones. If the Gorny Altai greenstones are to be compared with the island arc and the back-arc, the greenstones are expected to be associated with thick volcaniclastics or terrigenous turbidite. However, the Gorny Altai greenstones are overlain by micritic limestone. Similarly, the plume–arc interaction model has the same problem as arc and back-arc development model. If the Gorny Altai greenstones are generated in an arc above an accreted oceanic plateau, Groups 1 and 3 could be covered by micritic limestone and Groups 2 and 4 could be overlain by thick volcaniclastics or terrigenous turbidite. However, Groups 2 and 4 are in fact also associated with micritic limestones (Fig. 4).

7.5.4. Comparison with modern oceanic plateaus

Some oceanic plateaus show significant compositional heterogeneity. For example, basalts from the Caribbean and Gorgona plateaus have REE patterns ranging from LREE-depleted to LREE-enriched (e.g., Kerr et al., 1997). A small amount of OIB-like alkaline basalt with HIMU signature also occurs with tholeiitic basalts in the Solomon Islands (Tejada et al., 1996). Note that the Solomon Islands are a part of the exposed Ontong Java Plateau, and they are composed predominantly of chemically evolved but uniform tholeiitic basalts. The heterogeneity shown above requires distinct mantle sources with variable depletion and enrichment of trace elements (Kerr, 2005; Révillon et al., 2000; Tejada et al., 1996).

Basalts from several sites of oceanic plateaus in the Indian Ocean, such as the southern Kerguelen Plateau and the Naturaliste Plateau, show negative Nb–Ta anomalies (Mahoney et al., 1995; Neal et al., 2002). Parts of the Kerguelen and Naturaliste Plateaus were formed in proximity to rifted continental margins and that the continental lithosphere of eastern Gondawana remained above their mantle plume sources (Mahoney et al., 1995). Consequently, the negative Nb–Ta anomalies probably indicate assimilation of continental crust during magma genesis.

The Gorny Altai greenstones are likely to have formed in an oceanic plateau setting and their compositional heterogeneity is probably inherited from diverse sources. However, the tectonic setting is not likely to be similar to the Kerguelen and Naturaliste Plateaus, because the Gorny Altai greenstones were probably formed at mid-ocean, as constrained by field relationships.

The Ontong Java Plateau exhibits isotopic and chemical compositions similar to other oceanic basalts (i.e. no continental lithospheric signature) (Mahoney et al., 1993; Tejada et al., 1996; Fitton and Godard, 2004). However, a compositionally varied suite of mantle xenoliths occurs in Malaita, Solomon Islands (Ishikawa et al., 2004). A thermobarometric and petrochemical study on the garnet pyroxenite xenoliths suggests high-pressure melting residues of basaltic material were incorporated into peridotite (Ishikawa et al., 2004). The Hf–Nd isotopic compositions of garnet clinopyroxenite xenoliths are significantly decoupled from the oceanic basalt array, but are similar to that of the continental lower crust (Ishikawa et al., 2007). Thus, the basalts of the Ontong Java Plateau were likely derived from a source which contained recycled crustal material mixed into the deep mantle by subduction (Ishikawa et al., 2007).

In the plot of Th/Nb vs. Ti/Nb (Fig. 13), Groups 2 and 4 greenstones are found to be similar to the lower continental crust (LC). The Th/Nb and Ti/Nb ratios suggest that the Gorny Altai greenstones likely formed from a source which contained recycled crustal materials. Worldwide distributed granulite xenoliths considered to be lower continental crust show large range of $\varepsilon_{Nd}(t)$. For example, $\varepsilon_{Nd}(t)$ values of -9.4 to $+7.2$ are found for granulite xenoliths from
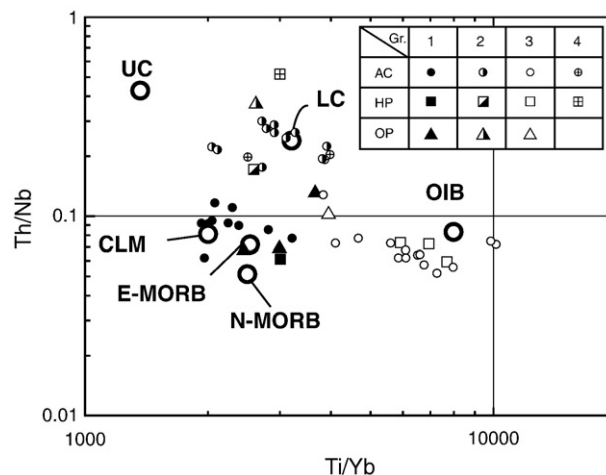
Fig. 13. Th/Nb vs. Ti/Yb diagrams for the Gorny Altai greenstones. UC = upper continental crust; LC = lower continental crust; and CLM = continental lithospheric mantle. Reference values of N- and E-MORB and OIB are from Sun and McDonough (1989). UC, LC and CLM is from Taylor and McLennan (1985), Rudnick and Fountain (1995) and McDonough (1990), respectively.

southeast China (Yu et al., 2003) and the values of -16.5 to $+11.3$ for the xenoliths from north Queensland, Australia (Stortz and Davies, 1989). Combined with trace element and Sr isotope compositions, Nd isotope compositions of the xenoliths are interpreted to result from assimilation and fractional crystallization of depleted-mantle-derived basaltic melt with continental crustal assimilates (Yu et al., 2003; Rudnick, 1990). With the assumption that the lower continental crust has 2.8 and 11 ppm of Sm and Nd, respectively (Rudnick and Fountain, 1995) and a depleted initial ε_{Nd} ($+8.5$—$+9.0$), $\varepsilon_{Nd}(t)$ of Groups 2 and 4 greenstones suggests that the crustal materials in a source region was 300–500 million-year-old at the time. The relatively young lower continental crust might be incorporated into the mantle and trapped by the plume without a long residence time. The difference between the erupted Ontong Java Plateau basalt and the Gorny Altai greenstones may be due to the different proportions of assimilated crustal materials involved in petrogenesis. The crustal signature of the Ontong Java Plateau was probably diluted by the extensive melting of surrounding mantle peridotites. The Gorny Altai greenstones, on the other hand, likely included more recycled lower continental crustal materials or melted less mantle peridotite. The plume responsible for the Gorny Altai greenstones may have been relatively cool and thus favored melting of a crustal component due to a lower melting temperature than the mantle peridotites. Also, the comparatively small amount of basalts indicates a lower degree of partial melting than the Ontong Java Plateau, and it may have contributed to retaining the distinct crustal signature.

8. Conclusions

The Gorny Altai greenstones occur as a coherent suite of an ophiolite complex and as blocks in the sedimentary or serpentinite matrix. The occurrence of the latter is similar to a typical chaotic-type accretionary complex that is formed when topographic highs are accreted at a subduction zone. The greenstones are directly overlain by micritic limestones or intercalated with micritic limestones without terrigenous materials. The geologic characteristics indicate that the greenstones were formed in shallow water in a mid-ocean environment and were subsequently tectonized and mixed either during or after the accretion. The Gorny Altai greenstones show heterogeneous compositions and variable degrees of subduction signature. The field relationship suggests that the greenstones with and without the subduction signature were formed at the same tectonic setting. We conclude that the most probable tectonic setting is an oceanic plateau generated by a mantle plume

containing recycled continental materials in the source region. If our model is correct, an important implication is that oceanic plateaus could be a significant component in the formation of an accretionary orogen.

Acknowledgement

Appendix A. Supplementary data

Supplementary data associated with this article can be found, in the online version, at doi:10.1016/j.lithos.2009.05.020.

References

Alt, J.C., Honnorez, J., 1984. Alteration of the upper oceanic crust, DSDP site 417: mineralogy and chemistry. Contributions to Mineralogy and Petrology 87, 149–169.

Bach, W., Alt, J.C., Niu, Y., Humphris, S.E., Erzinger, J., Dick, H.J., 2001. The geochemical consequences of late-stage low-grade alteration of the lower ocean crust at the SW Indian Ridge: results from ODP Hole 735B (Leg 176). Geochimica et Cosmochimica Acta 65, 3267–3287.

Buslov, M.M., Watanabe, T., 1996. Intra-subduction collision and its role in the evolution of an accretionary wedge: the Kurai zone of Gorny Altai, Central Asia. Russian Geology and Geophysics 36, 83–94.

Buslov, M.M., Berzin, N.A., Dobretsov, N.L., Simonov, V.A., 1993. Geology and Tectonics of Gorny-Altai. Novosibirsk. Guidebook for post-symposium excursion. The 4th international symposium of the IGCP project 283 "Geodynamic evolution of the Paleoasian ocean." UIGGM, SB, RAS, Novosibirsk, pp. 122.

Buslov, M.M., Sennikov, N.V., Iwata, K., Zybin, V.A., Obut, O.T., Gusev, N.I., Shokalsky, S.P., 1998. New data on the structure and age of olistostromal and sandy–silty rock masses of the Gorny–Altai series in the southeast of the Gorny–Altai, Anui–Chuya zone. Russian Geology and Geophysics 39, 801–809.

Buslov, M.M., Saphonova, I.Y., Watanabe, T., Obut, O.T., Fujiwara, Y., Iwata, K., Semakov, N.N., Sugai, Y., Smirnova, L.V., Kazansky, A.Yu., Itaya, T., 2001. Evolution of the Paleo-Asian Ocean (Altai–Sayan Region, Central Asia) and collision of possible Gondwana-derived terranes with the Southern marginal part of the Siberian continent. Geoscience Journal 5, 203–224.

Buslov, M.M., Watanabe, T., Saphonova, I.Yu., Iwata, K., Travin, A., Akiyama, M., 2002. A Vendian–Cambrian island arc system of the Siberian continents in Gorny Altai (Russia, Central Asia). Gondwana Research 5, 781–800.

Buslov, M.M., Watanabe, T., Smirnova, L.V., Fujiwara, I., Iwata, K., de Grave, J., Semakov, N.N., Travin, A.V., Kir, yanova, A.P., Kokh, D.A., 2003. Role of strike–slip faulting in Late Paleozoic–Early Mesozoic tectonics and geodynamics of the Altai–Sayan and East Kazakhstan regions. Russian Geology and Geophysics 44, 49–75.

Buslov, M.M., Watanabe, T., Fujiwara, Y., Iwata, K., Smirnova, L.V., Safonova, I.Yu., Semakov, N.N., Kiryanova, A.P., 2004. Late Paleozoic faults of the Altai region, Central Asia: tectonic pattern and model of formation. Journal of Asian Earth Sciences 23, 655–671.

Desrochers, J.-P., Hubert, C., Ludden, J.N., Pilote, P., 1993. Accretion of Archean oceanic plateau fragments in the Abitibi greenstone belt, Canada. Geology 21, 451–454.

Dobretsov, N.L., Berzin, N.A., Buslov, M.M., 1995. Opening and tectonic evolution of the Paleo-Asian Ocean. International Geology Review 35, 335–360.

Dobretsov, N.L., Buslov, M.M., Safonova, Y.I., Kokh, D.A., 2004. Fragments of oceanic islands in the Kurai and Katun' accretionary wedge of Gorny Altai. Russian Geology and Geophysics 45, 1381–1403.

Fitton, J.G., Godard, M., 2004. Origin and Evolution of magmas on the Ontong Java Plateau. In: Fitton, J.G., Mahoney, J.J., Wallace, P.J., Saunders, A.D. (Eds.), Origin and evolution of the Ontong Java Plateau. Special Publications 229. Geological Society, London, pp. 151–178.

Hollings, P., Wyman, D., 1999. Trace element and Sm–Nd systematics of volcanic and intrusive rocks from the 3Ga Lumby Lake Greenstone belt, Superior Province: evidence for Archean plume–arc interaction. Lithos 46, 189–213.

Hollings, P., Stott, G., Wyman, D., 2000. Trace element geochemistry of the Meen–Dempster greenstone belt, Uchi subprovince, Superior Province, Canada: back-arc development on the margins of an Archean protocontinent. Canadian Journal of Earth Sciences 37, 1021–1038.

Ishikawa, A., Maruyama, S., Komiya, T., 2004. Layered lithospheric mantle beneath the Ontong Java Plateau: implications from xenoliths in Alnöite, Malaita, Solomon Islands. Journal of Petrology 45, 2011–2044.

Ishikawa, A., Kuritani, T., Makishima, A., Nakamura, E., 2007. Ancient recycled crust beneath the Ontong Java Plateau: isotope evidence from the garnet clinopyroxenite xenoliths, Malaita, Solomon Islands. Earth and Planetary Science Letters 259, 134–148.

Isozaki, Y., 1997. Jurassic accretion tectonics of Japan. The Island Arc 6, 25–51.

Jahn, B.-m., 2004. The Central Asian Orogenic Belt and growth of the continental crust in the Phanerozoic. In: Malpas, J., Fletcher, C.J.N., Ali, J.R., Aitchison, J.C. (Eds.), Aspects of the Tectonic Evolution of China. Special Publications 226. Geological Society, London, pp. 73–100.

Jahn, B.-m., Bernard-Griffiths, J., Charlot, R., Cornichet, J., Vidal, F., 1980. Nd and Sr isotopic compositions and REE abundances of Cretaceous MORB (Holes 417D and 418A, Leg 51 and 53). Earth and Planetary Science Letters 48, 171–184.

Jahn, B.-m., Griffin, W.L., Windley, B.F. (Eds.), 2000. Continental growth in the Phanerozoic: evidence from Central Asian Orogenic Belt: Tectonophysics, vol. 328, pp. 1–227.

Jahn, B.-m., Windley, B.F., Natal'in, B., Dobretsov, N. (Eds.), 2004. Phanerozoic continental growth in Central Asia: Journal of Asian Sciences, vol. 23, pp. 599–815.

Jochum, K.P., Verma, S.P., 1996. Extreme enrichment of Sb, Tl and other trace elements in altered MORB. Chemical Geology 130, 289–299.

Kanazawa, T., Sager, W.W., Escutia, C., et al., 2001. Proceedings of the Ocean Drilling Program, Initial Reports 191. Ocean Drilling Program, College Station, TX. doi:10.2973/odp.proc.ir.191.2001.

Kerr, A.C., 2005. La Isla de Gorgona, Colombia: A petrological enigma? Lithos 84, 77–101.

Kerr, A.C., Tarney, J., Marriner, G.F., Nivia, A., Saunders, A.D., 1997. The Caribbean–Colombian Cretaceous Igneous Province: the internal anatomy of an oceanic plateau. In: Mahoney, J.J., Coffin, M.F. (Eds.), Large Igneous Provinces; Continental, Oceanic, and Planetary Flood Volcanism. Geophysical Monograph Series, vol. 100. American Geophysical Union, Washington, D.C., pp. 123–144.

Kovalenko, V.I., Yarmolyuk, V.V., Kovach, V.P., Kotov, A.B., Kozakov, I.K., Salnikova, E.B., Larin, A.M., 2004. Isotope provinces, mechanisms of generation and sources of the continental crust in the Central Asian mobile belt: geological and isotopic evidence. Journal of Asian Earth Sciences 23, 605–627.

Lee, C.Y., Tsai, J.H., Ho, H.H., Yang, T.F., Chung, S.L., 1997. Quantitative analysis in rock samples by and X-ray fluorescence spectrometer (I) major elements. Program with Abstracts of 1997 Annual Meeting of Geological Society of China, Taipei, pp. 418–420 (in Chinese).

Mahoney, J.J., Storey, M., Duncan, R.A., Spencer, K.J., Pingle, M., 1993. Geochemistry and geochronology of the Ontong Java Plateau. In: Pringle, M., Sager, W., Sliter, W., Stein, S. (Eds.), The Mesozoic Pacific Geology, Tectonics, and Volcanism. Geophysical Monograph Series, vol. 77. American Geophysical Union, Washington, D.C., pp. 233–261.

Mahoney, J.J., Jones, W.B., Frey, F.A., Salters, V.J.M., Pyle, D.G., Davis, H.L., 1995. Geochemical characteristics of lavas from Broken Ridge, the Naturaliste Plateau and southernmost Kerguelen Plateau: Cretaceous plateau volcanism in the southeast Indian Ocean. Chemical Geology 120, 315–345.

McDonough, W.F., 1990. Constraints on the composition of the continental lithospheric mantle. Earth and Planetary Science Letters 101, 1–18.

Miyashiro, A., 1973. The Troodos ophiolitic complex was probably formed in an island arc. Earth and Planetary Science Letters 19, 218–224.

Mullen, E.D., 1983. MnO–TiO₂–P₂O₅: a minor element discriminate for basaltic rocks of oceanic environments and its implication for petrogenesis. Earth and Planetary Science Letters 62, 53–62.

Neal, C.R., Mahoney, J.J., Chazey, W.J., 2002. Mantle source and the highly variable role of continental lithosphere in basalt petrogenesis of the Kerguelen Plateau and Broken Ridge LIP: results from ODP Leg 183. Journal of Petrology 43, 1177–1205.

Ota, T., Utsunomiya, A., Uchio, Y., Isozaki, Y., Buslov, M.M., Ishikawa, A., Maruyama, S., Kitajima, K., Kaneko, Y., Yamamoto, H., Katayama, I., 2007. Geology of the Gorny Altai subduction–accretion complex, southern Siberia: tectonic evolution of an Ediacaran–Cambrian intra-oceanic arc-trench system. Journal of Asian Earth Sciences 30, 666–695.

Pearce, J.A., 1996. A user's guide to basalt discrimination diagrams. In: Wyman, D.A. (Ed.), Trace Element Geochemistry of Volcanic Rocks: Applications for Massive Sulphide Exploration. Short Course Notes, vol. 12. Geological Association of Canada, pp. 79–113.

Pearce, J.A., Cann, J.R., 1973. Tectonic setting of basic volcanic rocks determined using trace element analyses. Earth and Planetary Science Letters 19, 290–300.

Pearce, J.A., Kempton, P.D., Nowell, G.M., Noble, S.R., 1999. Hf–Nd element and isotope perspective on the nature and provenance of mantle and subduction components in western Pacific arc-basin system. Journal of Petrology 40, 1579–1611.

Révillon, S., Arndt, N.T., Chauvel, C., Hallot, E., 2000. Geochemical study of ultramafic volcanic and plutonic rocks from Gorgona Island, Colombia: the plumbing system of an oceanic plateau. Journal of Petrology 41, 1127–1153.

Rudnick, R.L., 1990. Nd and Sr isotopic compositions of lower-crustal xenoliths from north Queensland, Australia: implications for Nd model ages and crustal growth processes. Chemical Geology 83, 195–208.

Rudnick, R.L., Fountain, D.M., 1995. Nature and composition of the continental crust: a lower crustal perspective. Reviews of Geophysics 33, 267–309.

Safonova, I.Y., Buslov, M.M., Iwata, K., Kokh, D.A., 2004. Fragments of Vendian–Early Carboniferous oceanic crust of the Paleo-Asian Ocean in foldbelts of the Altai–Sayan Region of Central Asia: geochemistry, biostratigraphy and structural setting. Gondwana Research 7, 771–790.

Salisbury, M.H., Shinohara, M., Richter, C., et al., 2002. Proceedings of the Ocean Drilling Program, Initial Reports 195. InOcean Drilling Program, College Station, TX. doi:10.2973/odp.proc.ir.195.2002.

Sengör, A.C.M., Natal'in, B.A., 1996. Paleotectonics of Asia: fragments of a synthesis. In: Yin, A., Harrison, T.M. (Eds.), The tectonic evolution of Asia. Cambridge University Press, Cambridge, pp. 486–640.

Sengör, A.C.M., Natal'in, B.A., Burtman, V.S., 1993. Evolution of the Altaid tectonic collage and Paleozoic crustal growth in Eurasia. Nature 364, 299–307.

Seno, T., Maruyama, S., 1984. Paleogeographic reconstruction and motion history of the Philippine Sea. Tectonophysics 102, 53–84.

Shervais, J.W., 1982. Ti–V plots and the petrogenesis of modern and ophiolitic lavas. Earth and Planetary Science Letters 59, 101–118.

Shervais, J.W., 2001. Birth, death, and resurrection: the life cycle of supra-subduction zone ophiolites. Geochemistry, Geophysics, Geosciences 2. doi:10.1029/2000GC000080.

Shervais, J.W., Kimbrough, D.L., Renne, P., Hanan, B.B., Murchey, B., Snow, C.A., Schuman, M.M.Z., Beaman, J., 2004. Multi-stage origin of the Coast Range ophiolite, California: implications for the life cycle of supra-subduction zone ophiolites. International Geology Review 46, 289–315.

Stortz, A.J., Davies, G.R., 1989. Metasomatised lower crustal and upper mantle xenoliths from north Queensland: chemical and isotopic evidence bearing on the composition and source of the fluid phase. Geochimica et Cosmochimica Acta 53, 649–660.

Sun, S.-S., McDonough, W.F., 1989. Chemical and isotopic systematics of oceanic basalts; implications for mantle composition and processes. In: Saunders, A.D., Norry, M.J. (Eds.), Magmatism in the ocean basins. Special Publications 42. Geological Society, London, pp. 313–345.

Taylor, S.R., McLennan, S.M., 1985. The continental crust: its composition and evolution. Blackwell Science Inc, Cambridge, p. 312.

Tejada, M.L.G., Mahoney, J.J., Duncan, R.A., Hawkins, M.P., 1996. Age and geochemistry of basement and alkalic rocks of Malaita and Santa Isabel, Solomon Islands, southern margin of Ontong Java Plateau. Journal of Petrology 37, 361–369.

Terleev, A.A., 1991. Stratigraphy of Vendian–Cambrian sediments of the Katun anticline (Gorny Altai). In: Khomentovskiy, V.V. (Ed.), Late Precambrian and Early Paleozoic of Siberia. UIGGM Publ., Novosibirsk, pp. 82–106 (in Russian).

Uchio, Y., Isozaki, Y., Ota, T., Utsunomiya, A., Buslov, M.M., Maruyama, S., 2004. The oldest mid-oceanic carbonate buildup complex: Setting and lithofacies of the Vendian (Late Neoproterozoic) Baratal limestone in the Gorny Altai Mountains, Siberia. Proceedings of the Japan Academy, Series B 9, 422–428.

Yang, J.H., Chung, S.L., Wilde, S.A., Wu, F.Y., Chu, M.F., Lo, C.H., Fan, H.R., 2005. Petrogenesis of post-orogenic syenites in the Sulu Orogenic Belt, east China: geochronological, geochemical and Nd–Sr isotopic evidence. Chemical Geology 214, 99–125.

Yu, J.-H., Xu, X., O, Reilly, Y., Griffin, W.L., Zhang, M., 2003. Granulite xenoliths from Cenozoic basalts in SE China provide geochemical fingerprints to distinguish lower crust terranes from the North and South China tectonic blocks. Lithos 67, 77–102.

Yuan, C., Sun, M., Zhou, M.-F., Xiao, W., Zhou, H., 2005. Geochemistry and petrogenesis of the Yishak Volcanic Sequence, Kudi ophiolite, West Kunlun (NW China): implications for the magmatic evolution in a subduction zone environment. Contributions to Mineralogy and Petrology 150, 195–211.

Zindler, A., Hart, S., 1986. Chemical geodynamics. Annual Review of Earth and Planetary Sciences 14, 493–571.